A THESIS SUBMITTED TO
THE GRADUATE SCHOOL OF NATURAL AND APPLIED SCIENCES
OF ÇANKIRI KARATEKİN UNIVERSITY

STUDY OF SOME PHYSICAL AND MECHANICAL PROPERTIES OF THE FLAME THERMAL SPRAY METHOD TO PRODUCE COMPOUNDS WITH (AL-WC) SYSTEM TO PROTECT TURBINE BLADES

IN PARTIAL FULFILLMENT OF THE REQUIREMENTS
FOR
THE DEGREE OF MASTER OF SCIENCE
IN
PHYSICS

BY

JALAL RIYADH NAYYEF NAYYEF

ÇANKIRI

2022

STUDY OF SOME PHYSICAL AND MECHANICAL PROPERTIES OF THE FLAME THERMAL SPRAY METHOD TO PRODUCE COMPOUNDS WITH (AL-WC) SYSTEM TO PROTECT TURBINE BLADES

By Jalal Riyadh NAYYEF NAYYEF

August 2022

We certify that we have read this thesis and that in our opinion it is fully adequate, in scope and in quality, as a thesis for the degree of Master of Science

Advisor **:** Prof. Dr. Hamit ALYAR
Co-Advisor **:** Asst. Prof. Dr. Salih Younis DARWEESH

Examining Committee Members:

Chairman **:** Prof. Dr. Mustafa Kemal ÖZTÜRK
Physics
Gazi University

Member **:** Prof. Dr. Hamit ALYAR
Physics
Çankırı Karatekin University

Member **:** Assoc.Prof. Dr.İlyas İNCİ
Physics
Çankırı Karatekin University

Approved for the Graduate School of Natural and Applied Sciences

Prof. Dr. İbrahim ÇİFTÇİ
Director of Graduate School

I hereby declare that all information in this document has been obtained and presented in accordance with academic rules and ethical conduct. I also declare that, as required by these rules and conduct, I have fully cited and referenced all material and results that are not original to this work.

Jalal Riyadh NAYYEF NAYYEF

ABSTRACT

STUDY OF SOME PHYSICAL AND MECHANICAL PROPERTIES OF THE FLAME THERMAL SPRAY METHOD TO PRODUCE COMPOUNDS WITH (AL-WC) SYSTEM TO PROTECT TURBINE BLADES

Jalal Riyadh NAYYEF NAYYEF

Master of Science in Physics

Advisor: Prof. Dr. Hamit ALYAR

Co-Advisor: Asst. Prof. Dr. Salih Younis DARWEESH

August 2022

The hardness test was carried out for both Porosity and adhesion strength at weight ratios % (5,10,15,20,25,30). Before conducting the sintering, the highest value of hardness was (153Hv) and the lowest value of porosity was (18%) and the highest value of adhesion strength was (23 MPa) were obtained at the percentage of reinforcement is (25%). Sintering at (1000°C) was carried out for two hours. Then the hardness, porosity and adhesive strength were retested, where we note the effect of sintering on each of the hardness, porosity and adhesion strength and the increase in the hardness value and adhesion strength to (178Hv) and (33 MPa), respectively. This test is resulted with a decrease in the porosity to (7%) and at the same reinforcement ratio of (25%). Also, X-ray diffraction (XRD) and scanning electron microscopy (SEM) were examined after sintering. You have the phases and these phases proved to us the improvement of the physical and mechanical properties of the material to reach the best at 25%. As for the SEM results, it was found that there was weakness and cracking in the coating layers at the low reinforcement ratios, while the physical and mechanical properties improved with the increase in the reinforcement ratios to reach the best at 25%.

2022, 73 pages

Keywords: Flame spray technology, SEM, XRD, Turbine blades

ÖZET

TÜRBİN KANATLARINI KORUMAK İÇİN ALEV TERMAL PÜSKÜRTME METODUYLA ÜRETİLEN (AL-WC) SİSTEMLİ BİLEŞİKLERİN BAZI FİZİKSEL VE MEKANİK ÖZELLİKLERİNİN ÇALIŞMASI

Jalal Riyadh NAYYEF NAYYEF
Fizik, Yüksek Lisans
Tez Danışmanı: Prof. Dr. Hamit ALYAR
Eş Danışman: Dr. Öğr. Üyesi Salih Younis DARWEESH
Ağustos 2022

Sertlik testi %(5,10,15,20,25,30) ağırlık oranlarında hem gözeneklilik hem de yapışma mukavemeti için yapıldı. Sinterleme işlemi yapılmadan önce en yüksek sertlik değeri (153Hv), en düşük gözeneklilik değeri (%18) ve en yüksek yapışma gücü değeri (23 MPa) donatı yüzdesinde (%25) elde edilmiştir. 1000 ° C'de sinterleme iki saat boyunca gerçekleştirildi. Daha sonra sertlik, gözeneklilik ve yapışma kuvveti yeniden test edildi, burada sinterlemenin her bir sertlik, gözeneklilik ve yapışma mukavemeti üzerindeki etkisini, sertlik değerindeki artışı ve yapışma mukavemetini sırasıyla (178Hv), (33 MPa) ve gözeneklilikte (%7) ve aynı takviye oranında (%25) azalma tespit edildi. Ayrıca, sinterlemeden sonra X ışını kırınımı (XRD) ve taramalı elektron mikroskobu (SEM) incelendi. Fazlar bize malzemenin fiziksel ve mekanik özelliklerinin %25'te en iyisine ulaşması için geliştirildiğini kanıtladı. SEM sonuçlarına gelince, düşük donatı oranlarında kaplama tabakalarında zayıflık ve çatlama olduğu, fiziksel ve mekanik özelliklerin ise donatı oranlarındaki artışla düzelerek %25'te en iyiye ulaştığı tespit edilmiştir.

2022, 73 sayfa

Anahtar Kelimeler: Alev püskürtme teknolojisi, SEM, XRD, Türbin kanatları

PREFACE AND ACKNOWLEDGEMENTS

It is a great pleasure to express my appreciation to the people who have contributed to completing this thesis. I would like to express my gratitude and appreciation to each of the advisors of this research, Prof. Dr. Hamit ALYAR and Asst. Prof. Dr. Salih Younis DARWEESH for their suggestion of this topic and for giving me a lot of valuable time and assistance while studying for the thesis. I would also like to thank them for their guidance and patience throughout my thesis. I am also very grateful to the faculty members of the Physics Department of the Faculty of Science in Çankırı Karatekin University. I would like to thank my mother and my father, who has always encouraged me and given me emotional support all time while writing this thesis. I would like to extend my heartfelt thanks to my brother Ali Riyad, my grandmother, my uncles, my aunts, and my friends for their support, encouragement, and assistance at all times in achieving my ambition.

Jalal Riyadh NAYYEF NAYYEF

Çankırı-2022

CONTENTS

LIST OF SYMBOLS

C.S	Particle size rate
D	The distance between the spray gun and the base
d_{av}	Average impact diameter adhesion adhesive force
d_{hkl}	The distance between the crystal planes
f	Shed pregnancy
Hv	Vickers hardness
P	Dry weight
t	The time it takes for the drop to reach the base
T	Time factor
v	Particle velocity
W_1	Hardness value
W_2	Saturated weight
W_3	Hanging weight
β	Curve width at mid-maximum intensity
θ	Diffraction angle
λ	The wavelength of the incident X-ray

LIST OF ABBREVIATIONS

ASTM	American standards for materials testing
EDS	Energy dispersive spectroscopy
FWHM	Full width at half maximum
HAP	Hydroxyapatite
HV	Hardness value
HVOF	High-velocity oxygen fuel
SEM	Scanning electron microscopy
TIG	Tungsten inert gas
XRD	Simulation body fluid
XRD	X-ray diffractometry

LIST OF FIGURES

LIST OF TABLES

1. INTRODUCTION

Most engineering failure happens for the mechanical parts because of the external circumstances surrounding the work of these parts. It begins with the change of colors, cracks, mechanical corrosion, and other superficial defects. Surface coating by increasing the thickness to a specified amount determined by the technique used is a critical way to increase the life of the parts. This can be done by selecting the appropriate engineering material for coating, which controls the surface defects of the mechanical parts mentioned above and thus achieves the required technical specifications, the most important of which are high hardness, oxidation resistance, and thermal stability (Holmes and Rahmel 1977).

The high developments in surface engineering technology-under, the effect of rehabilitation requirements expose to damage and put it back to the service, decrease the cost, enhance the performance and get technical specifications suitable to the application- led to considerable technological research in this field by thermal spraying processes to give protective cover with thickness between (50 μm –2mm) with the high performance of many coating materials that include metals, alloys, ceramic materials and composite materials for different industrial applications (Meetham *et al.* 2000).

The most critical engineering parts exposed to failure because of superficial defects are turbine blades in turbine engines because they are rotating parts that work in high temperatures with corrosive environments (Viswanathan and Dolbec 1987).

Turbine blades are made of superalloys because they have perfect mechanical and physical properties such as coefficient of thermal expansion, resistance to hot corrosion, good thermal stability, and resistance against oxidation that make them able to maintain their properties in long-term working conditions (Avner 1974, Ballard 1966).

All the manufactured turbine blades have operation life associated with standard working conditions. However, their work for long periods and exposure to high

temperatures distort dimensions, cause cracks or corrosion in the blades, or the occurrence of melting in some areas. So, how do rehabilitate these parts to work again with some actual technical specifications?

In order to answer this question, it is necessary to conduct an analytical study of those experimental processes from all sides, which can be summarized as follows:

It is reviewing the working concept of these turbine blades, which noted that they require special working conditions represented by high temperature and erosion resistance against gases. This, in turn, must be manufactured from a special alloy that keeps its good mechanical and physical properties under these conditions. The used engineering material suitable for these conditions in the manufacturing of turbine blades is the nickel-based Inconel alloy (Nabarro and De Villiers 2018, Mbaya and Hannafi 2021).

The rehabilitation process and return of the turbine blade to the service again after processing and protecting the surfaces from cracks or crevices are necessary with great economic feasibility because of the high cost of blades and the engineering effort consequences of replacing the blades from the turbine engine.

By reviewing the practical literature, we can find that the cladding process is implemented by one of the technology-based methods (Berndt *et al.* 2001, Davis 2001).

The criteria adopted for studying the efficiency of the cladding layer are tests of adhesion, porosity, oxidation resistance to high temperatures, thermal stability, and mechanical hardness, in addition to a microstructural test to observe the homogeneity of the coating layer and the absence of surface pores and cracks (J Talib *et al.* 2003, Jehn 2000).

The selection of composite Cermet materials includes oxides of ceramic materials with high melting points such as (Al2O3, TiO2, or Zr2O2) and added elements of iron

materials called Cermet. In recent years, researchers spent high efforts to use these composite materials widely in many electrical and thermal applications, which give good isolation properties at high temperatures, especially in jet engines, marine engines, and gas turbines (Vinson 1999). Composite materials are usually affected by the properties of materials included in their composition, including the matrix material and reinforcing phase. The matrix material is generally represented by the continuous phase in the composite material where it works on the cohesion and reinforcing materials and blind parts together to create a coherent modular system that can produce good mechanical properties, including the increase in durability and lightweight. Thus, the direction is to produce composite materials as an alternative for transitional engineering materials such as metals, alloys, and polymers. While the reinforcing materials reinforce the matrix, these ceramic materials may be ceramic, metals, or polymers with different shapes that may take the form of powders, fibers, or peels (Mondolfo 1985).

In recent ten years, producing composite materials has witnessed high development in producing composite materials reinforced by fibers, powder, or peels, especially by casting, powder technology, or thermal spray coating (Mondolfo 1985, Mondolfo 2013). Thermal spray techniques have an advanced position in coating processes (Mondolfo 1985). It allows the use of a wide range of materials, from materials with low melting points to materials with high melting points and composites, to obtain good physical and mechanical properties of the coating. These techniques are also generally considered the most widely used industrial means for external cladding for industrial requirements, especially for efficiently coating large pieces at high deposition rates. These techniques need high accuracy and control by the coating coefficients and circumstances such as material feeding rate, air force, and the distance between the spray gun and the base to get coatings with good adhesive strength and high structural and mechanical properties (Mondolfo 1985).

The current research deals with the process of manufacturing Cermet materials represented by the [AL2O3 + (Ni-al)] system using flame spraying technology and studies the effect of spraying variables on the final properties of the composite material when using different percentages of reinforcing materials to obtain high adhesion and

resistance coating layers used. This is done to rehabilitate turbine blades due to their properties in resisting oxidation at high temperatures and the ability to resist mechanical wear called (wear) (Mondolfo 2013). In addition to the introduction, previous studies, and research goal in the first chapter, the thesis includes three other chapters starting in the second chapter. It includes the essential concepts and theoretical principles of thermal spray in detail, the properties of thermal spray coating, simple ideas on nickel-based superalloys, and a summary of alumina, its phases, and applications. The third chapter addresses the practical side of preparing the composite materials and the most important physical and mechanical tests to reach the results. Chapter four consists of the research findings and discussion and ends with the conclusion and proposed recommendations for future studies.

Many studies and researches addressed the thermal spray coating with different types, the properties of resulting spray layers, and the possibility of controlling these properties by controlling the influenced spray coefficients. We will focus on the most critical research in coating methods.

Kucuk *et al.* (2000) used a plasma spray process by preparing a composite material of glass silica with nitride silica on steel bases and the analysis clarified with the x-ray diffraction the existence of the Si3 N4 phase in the coating as a reinforcement phase to the empty glass which gives high hardness to the coating (Ballard 1966). In the same year (2000), Tuominen *et al*. (2000) studied the effect of treatment by continuous Neodymium-YAG Laser after spraying using high-velocity oxygen fuel. After laser treatment and examination of the microstructure by optical microscopy and scanning microscopy, homogenization of the coating layer occurs, leading to increased adhesion to the layer (Li *et al.* 2002).

Li and Ohmori (2002) studied the relationship of porosity with the coating properties, including tensile strength and thermal conductivity, using copper plate (Al2O3) material and spray by plasma technique. The lamellar structure of the spray with binder material was the prevailing control variable in the sedimentation process. Also, the best spray distance was (100mm) with (13%) as the binder material rate (Kawakita *et al.* 2002).

Kawakita *et al* sprayed a layer of steel of (St.st 316L) type and coating on bases of the same steel (St.st 316L) with high-velocity oxygen fuel. In order to know its erosion in seawater under the effect of electrochemical erosion, they found that it is associated with each of the porosity and the existence of oxygen in the coating. Accordingly, the erosion takes a position between the tiny pores and borders of the sprayed particles on the base (Li *et al.* 2003).

Li *et al.* (2003) used the spray process with high-velocity oxygen. They studied the temperature generated by combustion, the fields of the velocity, and its effect on the movement and temperature of moving particles of different sizes. The study showed that the combustion pressure primarily influences the velocity of particles and that the temperature of particles is highly dependent on oxygen ratio and combustion fuel. It is found that the velocity of particles and temperature at the collision point is highly dependent on the particle size (Zhu and Miller 2004).

Zhu and Miller (2004) studied the thermal conductivity of the thermal barrier coating by using a plasma spray process of ceramic material ($ZrO_2 – Y_2O_3$) with an added binder (Ni-Al Cr Y) and treated by CO_2 laser with 3 KW energy. It is found that it decreases the thermal conductivity, reinforces the temperature resulting from the oxide group's existence, and enhances the coating's durability (Rocha *et al.* 2004).

Rocha *et al.* (2004) used electric arc spray by spraying an external layer of AL and an internal layer of AL-Fe-Cr on the steel base of type (387 G11). After putting the coating layer for 2.5 years in an atmosphere with a temperature of 550Cº and includes sulfur, oxygen, and carbon. It is found that porosity in the coating layer allows the penetration of corrosive conditions in the atmosphere, which induces the steady erosion of the steel layer. Also, it is found that the AL-Fe-Cr layer as the internal layer has not prevented the splits in the coating, and it also contributed to the internal erosion process (Sarikaya 2005).

Sarikaya (2005) researched the use of plasma spray of alumina Al_2O_3 on bases of steel of type (st. st 304 L). He studied the spray distance, base temperature, coating thickness,

and the surface roughness of coating on the resulted coating layer. It is found that these variables affect the hardness and porosity values. Also, it was found that the highest hardness and almost negligible value of porosity and roughness were at a distance of 12 cm (Darweesh *et al*. 2019).

The flame spray using Cermet composite material based on alumina material and different ratios with a metallic binder of (Ni-Al). It has been sprayed on Inconel alloy bases after preparation. It was found that the best ratio of binder material was 50%. Also, the obtained values of porosity and hardness are affected by the suitable thermal treatment of samples. The microstructure results give diffusion and homogeneity status with interconnection between components of coating material (Meetham *et al.* 2000).

Chaithanya (2007) used plasma spray (L Ni – A) material on medium carbon steel and copper bases. The coating properties such as porosity, hardness, tensile strength, and microstructure checking have been studied. It was found that the best spray energy was 20kw with the best adhesive values, and it was higher for steel than copper. Also, it is found that the microstructure is affected by the spray energy and that the coating is more complex than the spray bases. The corrosion rate is highly affected by particles' angle and collision velocity (Grewal *et al.* 2013).

Tarasi *et al*. (2008) sprayed Wt with 8% alumina mixed with yttria-stabilized zirconia; the effects of spray process coefficients on microstructure properties, including cracks, porosity, and sedimentation rate, have been studied. The temperature and velocity of particles were studied, and it was found that the thermal diffusivity of coating (an essential feature for thermal barriers) is not associated with whether the coating includes porosity. Also, the relationship of porosity with velocity is an inverse relationship. Whenever the velocity of particles is increased, the porosity will be decreased, and the decrease of porosity has led to increased hardness (Tarasi *et al.* 2008).

Al-Taha (2009) studied the high-velocity oxygen fuel spray by spraying the powder of Diamalloy 1005 mixed with WC powder on the bases of type 304 and used a laser of type CO2 for thermal treatment. The metallurgical properties of coating and

composition method by scanning microscope were studied in addition to the tensile and corrosion resistance. It is found that WC particles increase and decrease temperature and increase the levels of tensile and stress. After treatment by laser, it is found that after treating by laser, the corrosion resistance of the coating increases (Al-Taha 2009).

Patterson (2008) studied spraying the (Co - Ni - Cr - AL – Y) layer with plasma. The coating layer was oxidized at 1124 C ºfor (1, 6, 50, 100, and 300) hours to test the internal oxidization and its relationship with thermal conductivity and thermal diffusion coefficient as a function of oxide. The scanning microscope has been used to check the existence of oxide. It is found that the thermal conductivity of the coating layer is decreased by increasing the internal oxidization. Also, the diffusion coefficient has been measured at the thermal range (100 – 500) Cº, decreasing by increasing the internal oxidization within the range. It is found that the internal oxidization has less thermal expansion coefficient than metal coating (Patterson 2008).

Starosta (2008) used a flame spray of (Ni-AL) material on a base of steel type (st 45). It is found that increasing aluminum in coating increases the value of hardness and also found that the corrosion potential energy value is affected by the accurate composition and chemical composition of the coating. In addition, the study showed that increasing the aluminum rate decreases the corrosion energy despite increasing the porosity and found that the porosity rate of torch spray is larger than plasma spray (Starosta 2008).

De Silva (2010) studied the spray of yttria-stabilized zirconia by plasma, and the alumina was added by different mixing ratios and sprayed again. The addition of alumina has decreased the isolation of (YZS) material. The results showed that (YZS - Al2O3) material gives low thermal conductive values compared with (YZS) material and the reason is the increase in the porosity values of (YZS) material (De Silva 2010).

Al-Shehri (2011) used a high-velocity oxygen spray process by spraying Diamalloy 4010 powder, affected by wear, and Diamalloy 2002 powder, affected by corrosion and wear. It is found that the resulted coating from Diamalloy 2002 material gives higher hardness than Diamalloy 4010 material. This is due to the existence of WC in the

composition of the material. The tensile strength test leads to cracks forming beside the deep cracks, increasing the concentration of local stress, which leads to increased intensity under the tensile load (Al-Shehri 2011).

The binary system (Al-%WC) has been used to get reasonable physical, mechanical and structural properties suitable for turbine blades and oil pipelines, where aluminum is characterized by softness, ability to beat and tow, relatively stiffness, and corrosion resistance. In addition, Tungsten carbide is characterized by high hardness, resistance, and wear. Therefore, adding Tungsten carbide will enhance the nickel properties, and these turbine blades are usually used in high pumping electric power stations; thus, they corrode with time.

2. THEORETICAL SECTION

This chapter is interested in studying in detail the coatings and types of coating, especially by spraying and for each type of thermal spray and the mechanism of coating deposition in addition to the properties of thermal spray represented by microscopic structure, porosity, hardness, adhesion, and the relationship of each one of them with coating.

2.1 Thermal Spray

The thermal spray began in 1990 by a Swedish engineer (M.U. Schoop), where he was melting lead and tin wire using oxygen-acetylene (Zhu and Miller 2004). Between (1909-1921), there were twelve techniques based on (oxy-acetylene) torch as a thermal source, but it was limited to spraying the metal and ceramic materials with low melting points. At the end of the thirties, the first electric arc technique as a temperature source was used to melt the coating materials. Also, in 1955, the first plasma spray gun was produced, and it was in space applications (Rocha *et al.* 2004, Sarikaya 2005, Darweesh *et al.* 2019).

Finally, the thermal spray is a surface process technique by depositing metallic or non-metallic materials on molten or semi-molten material on previously prepared bases for coating and through which the material heats up and precipitates to form the coating on the base. Each process in this group is characterized by a method or point through which the material is treated and the change which occurs during the process (Grewal *et al.* 2013, Tarasi *et al.* 2008).

2.2 Scheme of Production Coating Techniques

There are many techniques to produce overlapping and non-overlapping materials, and they are classified based on the used thermal source to melt the coating material into two types which are chemical and electrical. The electrical includes plasma spray, and

electric arc spray, while the chemical includes detonation spray, high-velocity oxygen spray, and flame spray (Figure 2.1).

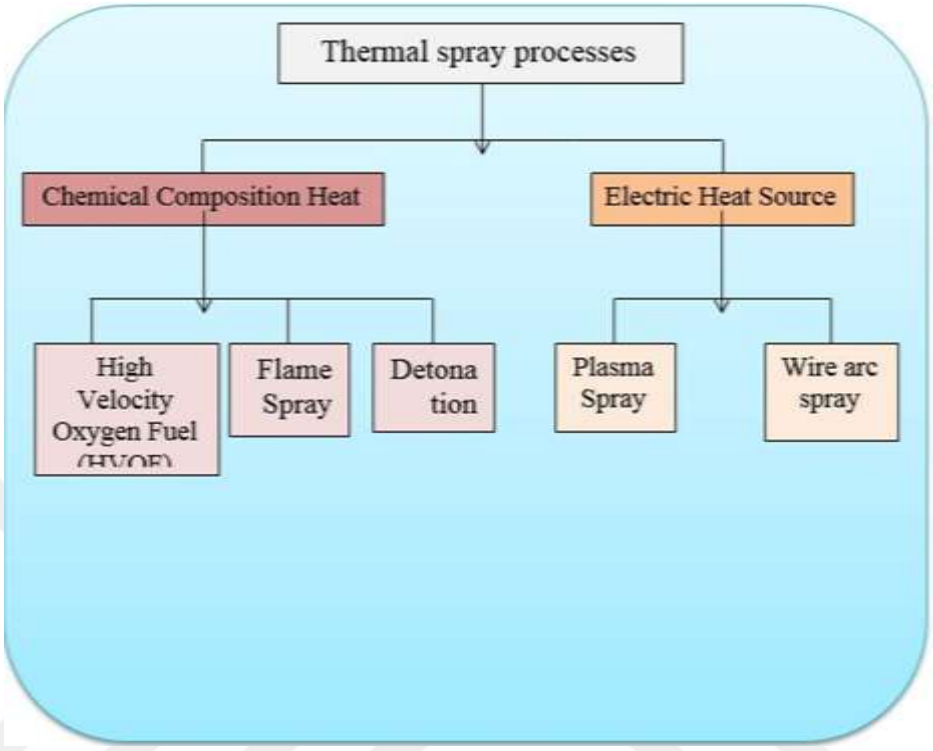

Figure 2.1 The techniques of coatings production (Chaithanya 2007)

2.3 The Base of Thermal Spraying Process and Types

Materials used in the thermal spray are varied; they may take the form of powders, wires, or bars and then be fed to the flame stream. At the same time, the kinetic and thermal energy of the torch can be produced whether from the mix of gaseous fuel and oxygen or by using an electrical energy source based on the source of energy. The coating materials are usually in their solid status, and they heat by gas combustion path such as flame spray or electrically by electric arc spray or plasma where it heats up and ionizes by a torrent of gases (Al-Taha 2009, Patterson 2008).

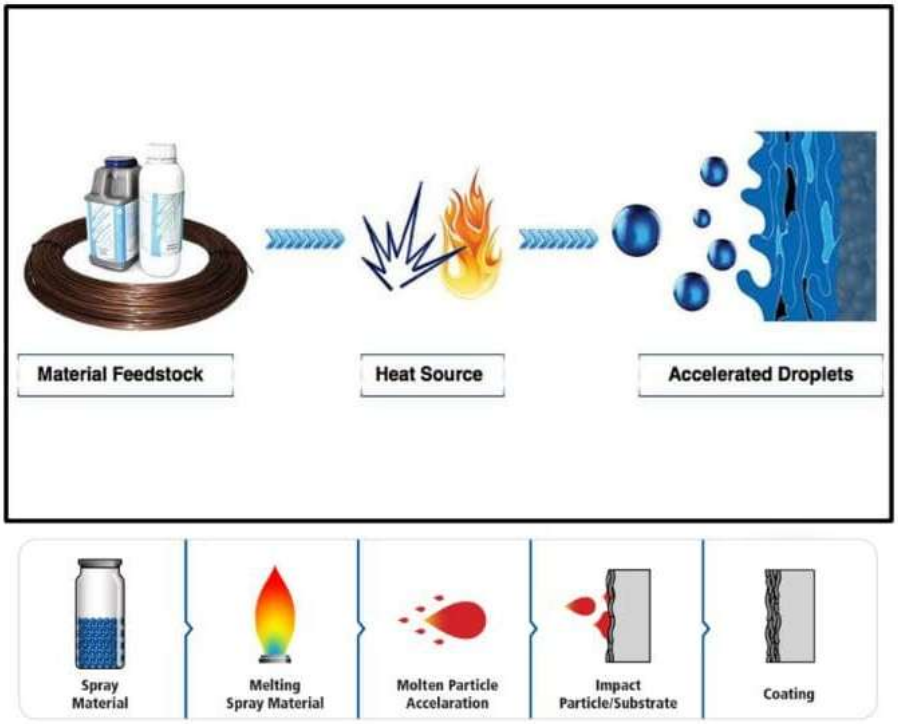

Figure 2.2 The stages of the spraying process (Starosta 2008)

It is constituted by the material prepared for spraying or coating, transformed to the melting status, and sprayed with fine granules and precipitate with high velocity towards the base surface by gas pressure (Figure 2.2). When it reaches the base, it flattens and finally adheres to the base. During the spraying process, the coating is constructed from the lamellar structure by quick freezing of melting or precipitated plastic droplets to the base (De Silva 2010). The thermal spray technique can be used in cladding metals, their alloys, ceramic materials, polymers, and thermal resistant metals (Al-Shehri 2011). Examples of those materials are (tungsten and molybdenum) and on a wide range of bases starting from bases with low melting points and ending with bases with high melting points (Martengo *et al.* 1987).

2.3.1 Flame spray

Flammable gas is used as a thermal source for melting the coating material in the flame spraying process. As shown in Figure 2.3 and Figure 2.4, the torch it results from flaming any fuel such as hydrogen, acetylene, or propylene with air or oxygen (Das

2007). At the same time, the coating materials used in this technique may be powder, bars, or wires. Also, the spray gun used in this technique is designed to fulfill this purpose and includes pathways for combustion gasses fuels where in case of using the powder, the combustion is out of the gun, and when using the wires, the combustion inside the spray hole (Spray 2004, Abkenar 2007).

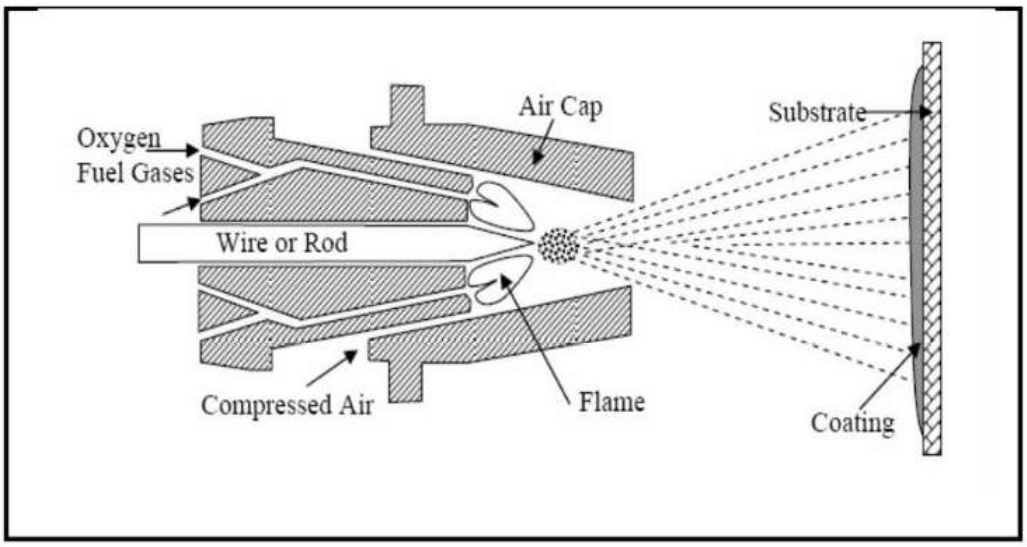

Figure 2.3 The spray process by wires

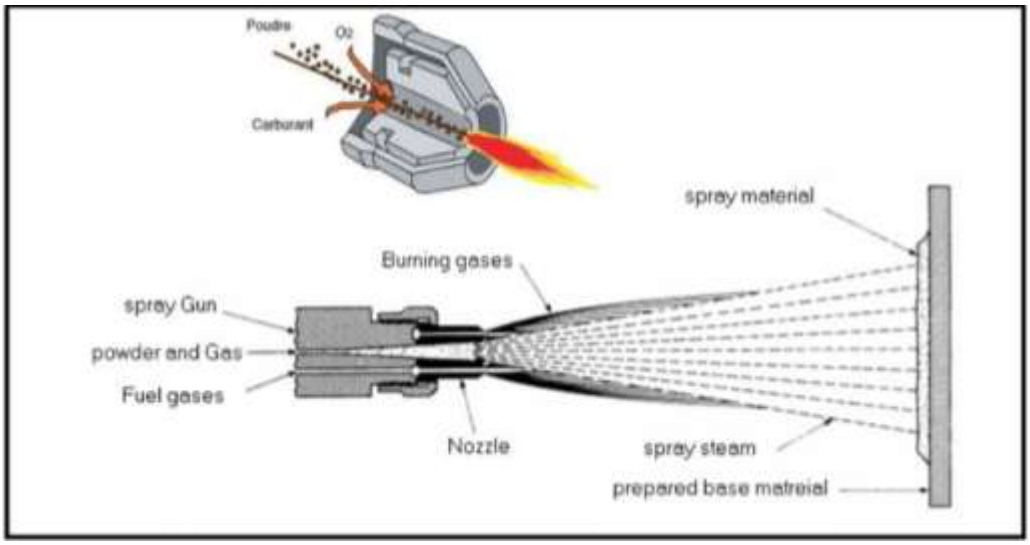

Figure 2.4 The spray process by powder (Gerdeman *et al.* 2012)

The flame temperature changes from (3000 Cº-3350 Cº) with a quick change in velocity from (80-100) m/s because of the pressure of combustion gases. The primary variables of spray in the torch system are (the coating material, feeding mechanism, gas fuel, air pressure, and distance from the goal). The binding strength is always about (15 Mpa) for ceramic coating, but it is higher with metal coating and about (30Mpa) and access to (60 Mpa) with (Al-Ni) coating. This spraying process heats the base (Das 2007, Spray 2004).

2.3.2 Electric arc spray

The cost of this technique is low because it depends on the use of electrical energy only without the need for expensive gas and constituting the coating electrically only because the thermal source is obtained from two conductive wires electrically charged with opposite charges of the coating material. They are electrically usable electrodes with two opposite charges of the coating material (Das 2007).

The melting thermal is generated due to passing a high current (50A-650A) between these two wires. The generated electric arc from the wires works on the two coating wires and thus molten the atomizes and reaches the base (Substrate) by compressed gas such as inert gases including nitrogen, argon, and the air (Figure 2.5). The conductive wires can be manufactured from pure metals or alloys, and electric spray has many properties such as a high ratio of sedimentation, low base temperature, low cost, and need for low energy (Das 2007, Beg 2020, Darweesh *et al.* 2019).

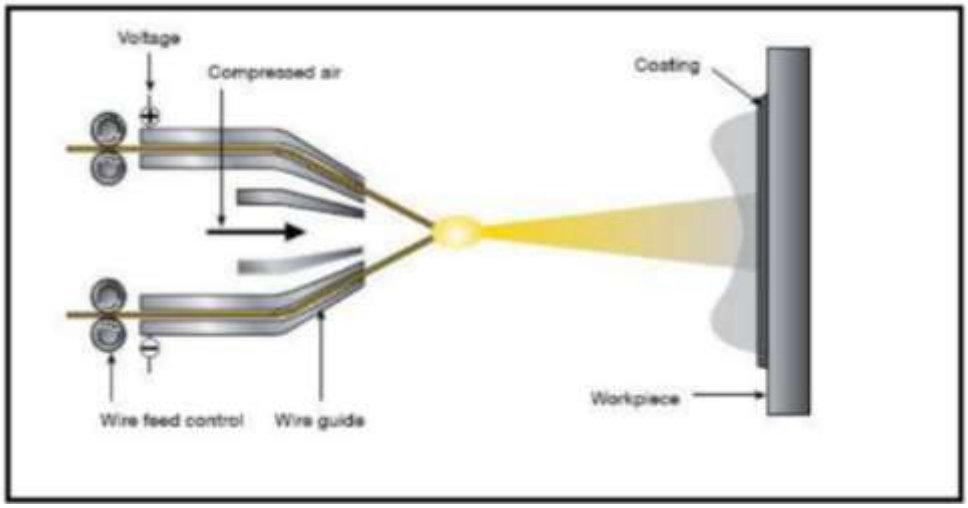

Figure 2.5 The electric arc spray process

2.3.3 Plasma spray

The name plasma spray came from using an electric arc as a thermal source to heat the gasses to reach (10000 Cº). The mix of gases disintegrates to equal ratios of free electrons and positive ions, and thus the plasma status is generated. Sometimes the temperature reaches (15000 Cº) (Satapathy 2005). In order to increase the temperature, secondary gases such as hydrogen-helium are added to the plasma. These gases raise the ionization voltage status and thermal content of plasma; therefore, the temperature is raised under a low level of energy (Das 2007).

This technique is widely operated on materials, excluding the disassociated materials before accessing the melting point or materials with a slight difference between the melting point and boiling point. The electric arc is constituted in this technique between the anode electrode and is a cylinder made of copper and constantly cooled by water (Figure 2.6). Between cathode electrode is made of tungsten material and located at the copper cylinder back, while the power port is coated. It locates at the front of the copper cylinder or near the flame exit (Satapathy 2005).

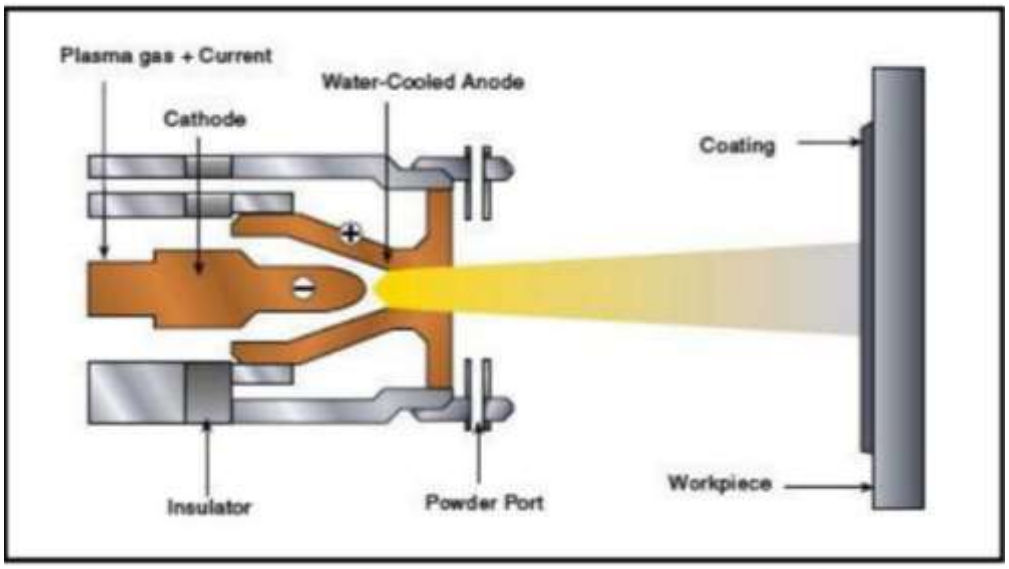

Figure 2.6 Plasma spraying process

The bonding strength of ceramic coating in the case of plasma spray is about (15-25) Mpa, and for metal coating, sometimes it reaches (70 Mpa), and because the velocity of droplets is high, the porosity is less where it is surrounding between (1-7) %. It is lower than the porosity obtained from the torch spray process (Das 2007).

2.3.4 Detonation spray

During this process, a mix of oxygen and acetylene gases is prepared and fed by a tabular pipe closed from one of its ends. In order to prevent the possible reverse combustion, the cover of each nitrogen gas allows covering the gas inlets. At the same time, the previously put quantity of coating powder is pushed to the combustion chamber. Combusting a set of gases generates a high shock wave (detonation wave). Later, the gas vapor diffuses, and the velocity of this wave may reach 3500 m/sec (Abkenar 2007, Heimann 2008).

Waves are heated up, and the coating material is precipitated through the pushing pipe to the base with a velocity reaching 120m/sec. Nitrogen batches are pushed to clean the pushing pipe after each detonation. As shown in Figure 2.7, when the high kinetic energy of the hot coating particles collides with the base, it produces a solid and dense

coating while the bonding strength to the base reaches (140Mpa) and the porosity ratio is between (0.25-1) (Das 2007, Spray 2004, Heimann 2008).

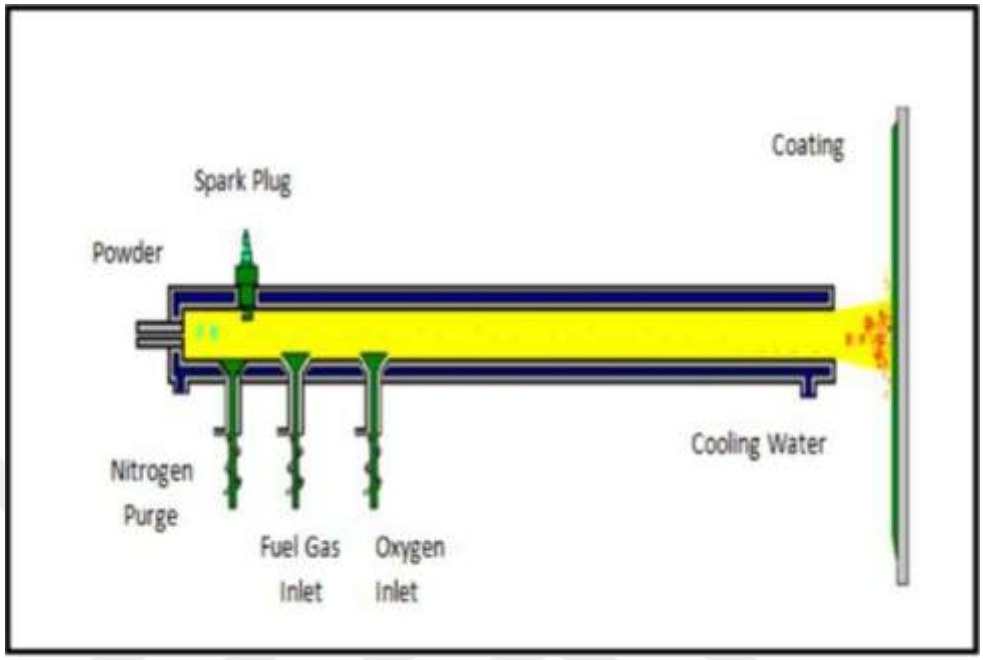

Figure 2.7 Detonation spray process

2.3.5 Spray by high-velocity oxygen combustion

This technique is considered one of the spray processing techniques and has gradually developed during the last two decades because its use was increased in surface engineering. It has been developed to resist wear in different fields, especially aerospace (Surmenev 2012, Allen *et al.* 2019). The base of the process is the combustion of fuel gas such as acetylene with oxygen in the combustion chamber, and the resulted combustion is under high pressure (3-10) bar (Figure 2.8). The velocity of generated vapor from the torch reaches 2000 m/sec. Due to the high combustion velocity, the particles' velocity is between (400-650) m/sec. As well as, the porosity of spray in this method is less than (1%), and because of the high velocity of collision, the resulting coating is highly dense (Das 2007).

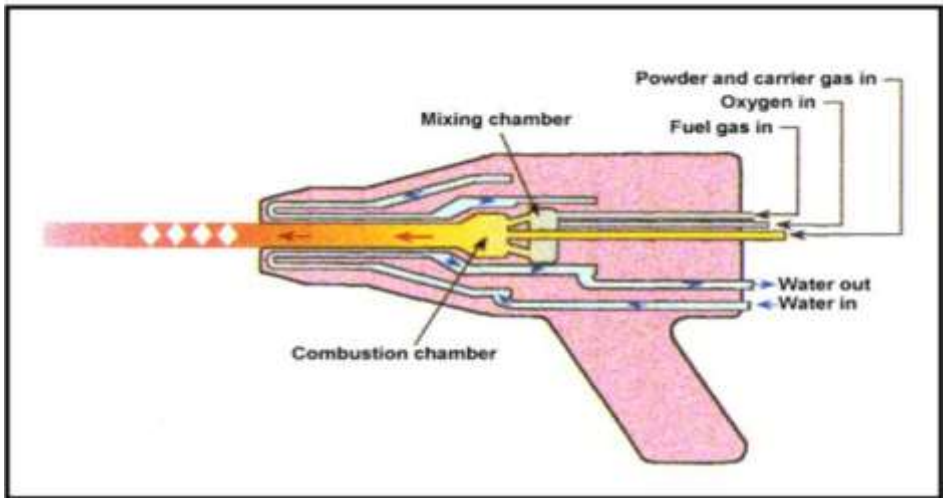

Figure 2.8 The process of spray by high-velocity oxygen combustion (Liu *et al.* 2021)

2.4 Comparison between Different Flame Spray Techniques

Table 2.1 Comparison between different flame spray techniques

Flame Spray	**Arc Spray**	**Plasma Spray**	**Detonation Spray**	**HVOF**
Acceptable adhesion strength	Acceptable adhesion strength	High adhesion strength	Very high adhesion rate	High adhesion rate
Medium porosity	Relatively low porosity	Low porosity	Very low porosity	Low porosity
Low cost	Low cost	Relatively high cost	High cost	High cost
Accompanied by heat transfer to the base	It is not accompanied by heat transfer to the base	It is not accompanied heat transfer to the base	It is not accompanied heat transfer to the base	It is not accompanied by heat transfer to the base
High sedimentation rates	High sedimentation rates	High sedimentation rates	Fewer sedimentation rates	Les sedimentation rate
Material limitations	Material limitations	Material limitations	Wider range	Wider range
High surface roughness	Less surface roughness	Low surface roughness	Less surface roughness	Less surface roughness
Low noise rate	Low noise rate	High noise rate	Very high noise rate	High noise rate

It is clear from the Table 2.1, that each technique has advantages and disadvantages, and the plasma spray technique is considered the best practice technique for producing homogeneous coatings with good psychical properties. Due to the lack of thermal spray devices for this technique, it has been reported to flame spray in preparing the sample of coatings in our research.

2.5 The Mechanism Forming of Thermal Spray Coatings

The coating techniques are evaluated by the range of protection provided by any coating technique during the testing processes. In order to know and develop the properties of the coating, it is necessary to understand its precise composition, which depends on the coating composition process (Sahab 2008). The coating layers of the thermal spray process are constituted from the collision of molten drops by the substrate, flattened and frozen to give lenticular. It is a dominant adjective for this type of coating. The previously frozen drops can be noticed, which tend to backtrack from the base. Therefore, it works to weaken the coating (Hafiz Abd Malek *et al.* 2013). While the spray occurs in the air, a layer of oxide is composed around the molten drops, and this influences the bonding of the coating (Figure 2.9). So, it is necessary to control the spray parameters which affect the coating composition process against the fully melting of coating material and the speed of drops, temperature, and size (Samal 2017).

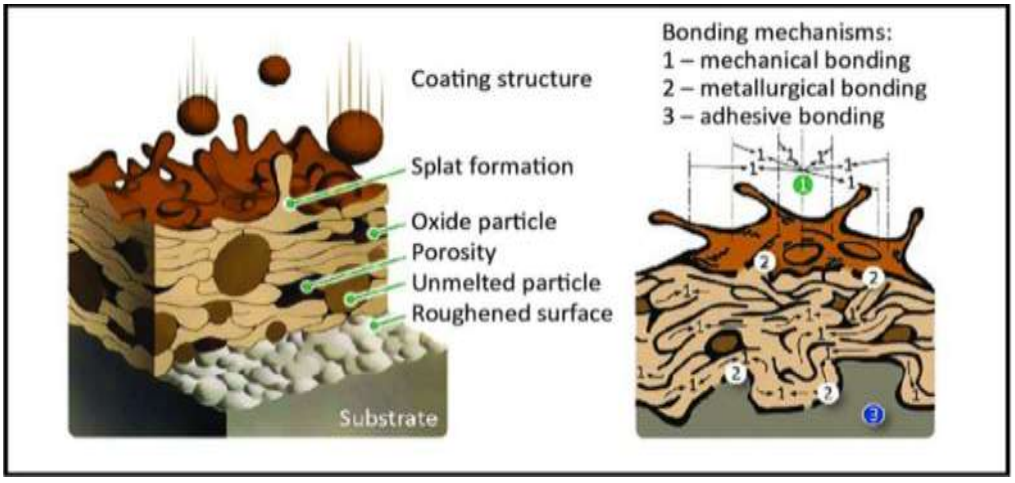

Figure 2.9 The thermal spray composition diagram

The oxidization layer surrounding the drop will be broken on the surface when the drop hits the base because of the oxide fragility (Samal 2017). The continuity of drops landing on the base and accumulating above each other with an average reaching one million drops per second relies on the area to be sprayed and the speed of gun movement. The thermal coating layers are composed of thickness between 10 μm and several centimeters, enough to be raised from the base and treated as the original material (Bulk) (Malek *et al.* 2014).

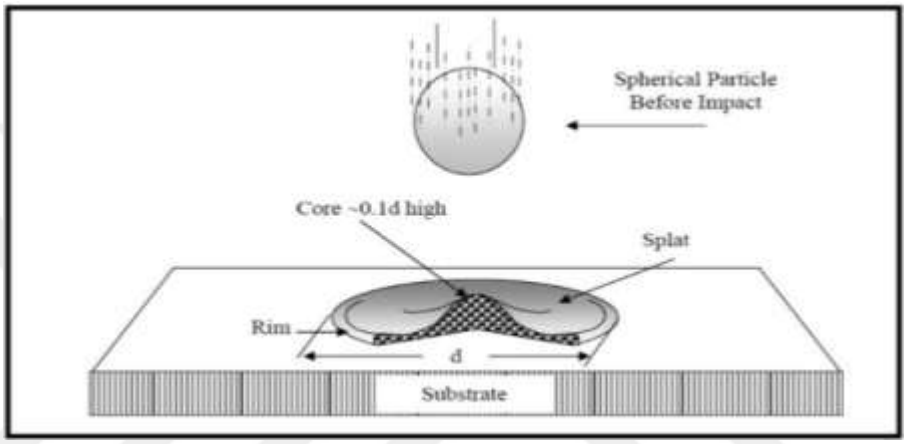

Figure 2.10 The collision of the drops with the base (Vardelle *et al.* 2016)

The collision mechanism of coating material drops on the base is summarized as follows: during the drops collision with the base surface, it flattens and flows in the form of the disk, as shown in Figure 2.10 and Figure 2.11, at the collision moment, the first connection of the drop with the base occurs at the core region, and then the temperature flows to the base. The unfrozen liquid of the drops will flow in a direction parallel to the base surface, far from the core. In the end, it hardens in the form of raised frame (Turunen 2005). While in the case of drops collision very quickly with the base, the liquid from the core will disintegrate to the outside to compose many tiny drops. This means that the drops here take different shapes (Dorfman 2002).

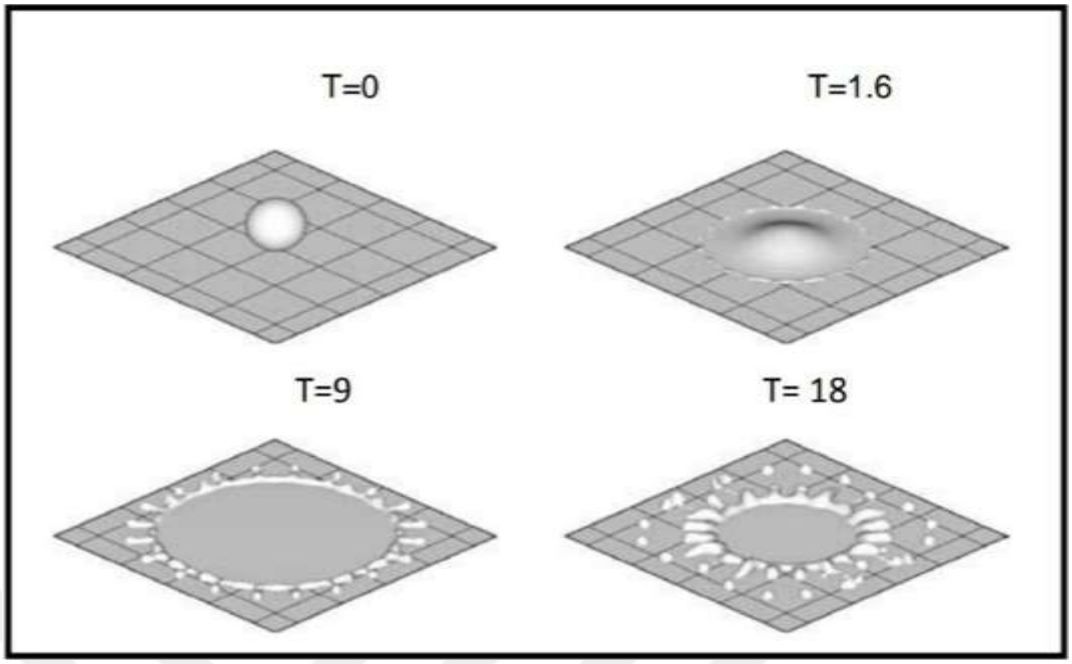

Figure 2.11 The shapes of drops at the collision (Chaithanya 2007)

Where T in Equation (2.1) is the time and it is equal to

$$T = \frac{tv}{D} \tag{2.1}$$

Where D is the distance between the spray gun and the base, v is the velocity of particles, and t is the time consumed by the drops to the base of what is called Fly Time.

2.6 The Temperature of the Particles at the Collision

The molten particles at the collision with the substrate (or layer previously precipitated) transform into sheets. The transformation process is associated with deformation and hardening processes, and this, in its turn, depends on many factors such as:

- The velocity, size, and phase content (completely liquid, partially liquid, etc.) of particles at the collision;
- The properties of particulate materials in liquid status (viscosity, surface tension, etc.);

- The ability of substrate hydration by the liquid particles.
- The substrate temperature.
- The roughness of the substrate.

The solidification and deformation processes occur at one time or more. The temperature at the front of a particle with the substrate during the collision, called contact temperature, influences the plate adhesion and, therefore, the adhesion of coating with the substrate. The adhesion mechanisms are probably, mechanical anchors and less likely mechanical bonds. The temperature in the structure of the particles, which can be measured currently using high-quality and sensitive sensors, affects the accurate structure of the coating. Firstly, and before everything, its development with time determines the solidification of material and cooling rates which affect the composition of crystal phases and size (Voorwald *et al.* 2005).

2.6.1 Particle deformation

Particle deformation relates to its solidification and is considered the fundamental problem in thermal spray. This problem is significant for the following reasons:

Deformation is independent of how the particle is fastening before the collision and heats up, which means that it is independent of the spray method. What is essential is the velocity at the effect and phase content of the particle (and, to some extent, the distribution of temperature inside the phases) at the effect point.

Lamellar microstructure, the feature of sprayed coatings, resulted from the deformation of the particles. The exception of this base is the hanging and sprayed coating by solution (Hotea *et al.* 2008). These coatings include microstructure which may include slightly deformed particles. Currently, hollow particles and other features are extensively studied.

Finally, the development of numerical and experimental tools currently allows the analysis of problems associated with deep deformation. Therefore, the last decade has created a fortune of theoretical and experimental data.

2.6.2 Particle temperature at impact

The coating adhesion determines the temperature in particles during the solidification with the substrate. On the other hand, the kinetic of solidification and cooling is determined by the size of the crystal. The last one influences many mechanical and electrical properties of the coating (Figure 2.12). Currently, rapid pyrometers can be used in the experimental determination of the temperature evolution of plate annealing and cooling on a substrate (Voorwald *et al.* 2005).

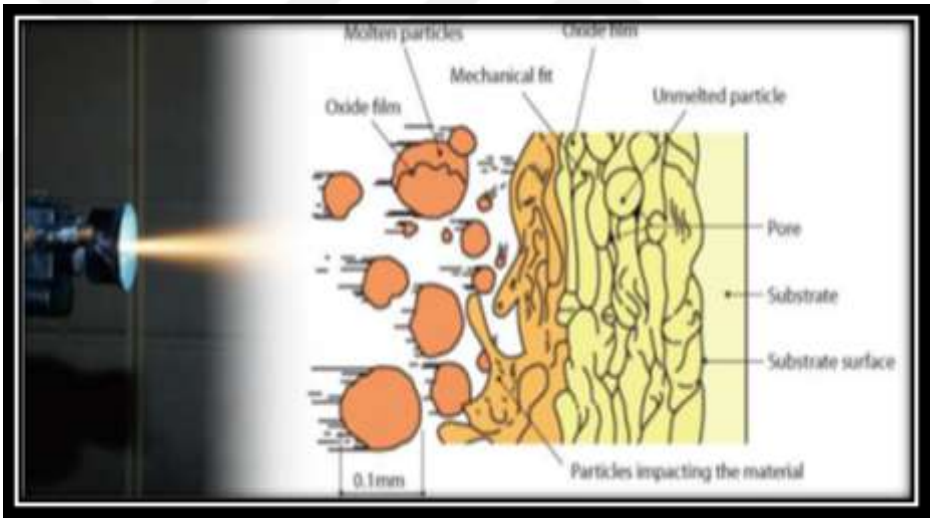

Figure 2.12 Particles effect the material

2.6.3 Adhesion mechanisms

The most precise and standard mechanism for the adhesion of coating by spray is the mechanical installation of slabs to substrate irregularities, as shown in (Figure 2.13). These substrates are caused by sandblasting or other methods to prepare the substrate before spraying (Ahmed *et al*. 2020). The hem is banded when solidified with the substrate by the strength resulting from liquid contraction. The touching points are

sometimes called the welding points (Lee *et al.* 2019) or active areas (Łatka *et al.* 2020) and correspond with a small part of the pumping area (20-30) % (Anupam *et al.* 2020, Bai *et al.* 2004). the adhesion of coating enhances if the active area becomes more extensive. Therefore, an increase in substrate temperature may promote the formation of such circles, which in turn must enhance the adhesion.

1. Low cooling influence.
2. Thermal contact resistance.

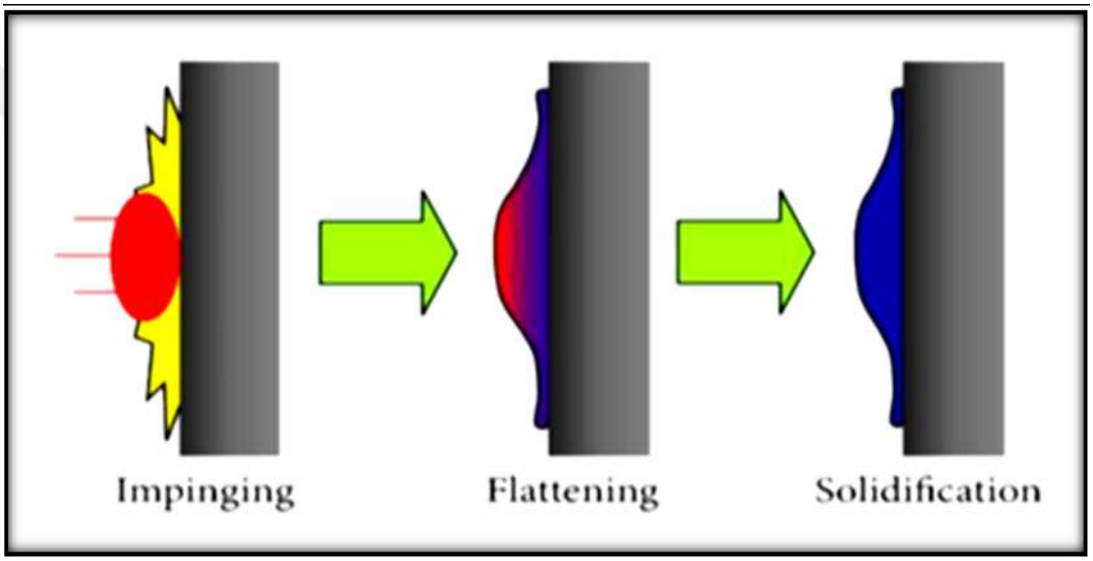

Figure 2.13 Mechanical installation for circles on the irregularities of the substrate surface active areas

Mechanical installation for circles on the irregularities of the substrate surface Active areas are decreased through the following:

- Oxides in the coatings of metals and alloys.
- Air or gases are the solute factor in liquid molecules “during the flying.”
- Air or pores fully by gas are surrounded because of the access of particles to the substrate.

Inside the active regions, the adhesion can be achieved by the following mechanisms:

- Physical interaction.
- Metallic interaction
- Other types of interactions

Solidification is a unique mechanism that may occur if the candidate material has the same or similar crystal structure (Voorwald *et al.* 2005).

2.7 Conditions of Thermal Spray Process

2.7.1 Substrates preparation

The thermal spray process requires a clean and rough surface and is free of pollutants such as oxides, fats, and impurities resulting from the roughing process. The purpose of surface preparation is to obtain high adhesion for the coating layer to the base, where the adhesion is an indicator of the success of the thermal spray process, and the purpose of roughing is to create sharp angles and protrusions to increase the mechanical bonding with the base. This means that rough is considered installation mode, and there are many methods for roughing, including grit blasting, threading, and grooving. When the drops hit the rough surface, they flatten to form splats that are mechanically intertwined with the base (Yin *et al*. 2019, Satapathy 2005).

1. Grit Blasted Method

It is one of the standard methods due to its ease of use and low cost, and this method is widely used to prepare the surface samples of thermal spray processes, especially the large particles. The base work of this method depends on pushing grits with sharp edges with high solidification, such as silicon carbide, aluminum oxide, or slag iron by compressed air to the base to be roughened. This process depends on many factors, such as the compressed air and the distance between the base and grit exit hole (Rybin *et al.* 2021, Matthews *et al.* 2008).

2. Rough Threading

The base of this method is to roughen the surface with a sharp tool that works to make threads by the depth of (0.7-09) mm and with a number (10-15) threads per centimeter and cutting angle (50°-70°) for the cylindrical parts. This method is commonly used in preparing bases with cylindrical shapes, and it is not used in preparing the bases of large pieces due to its slowness (Rybin *et al.* 2021, Matthews *et al.* 2008).

3. Groove Method

This method is different from the previously mentioned methods as the ends of grooves formed by this method are in the form of an arc, which means that the probability of crack formation is weaker. Therefore, it can be used to prepare heavy parts surfaces and parts exposed to high fatigue stresses (Matthews *et al.* 2008).

4. Arc Method of Preparation

This method roughens the high hardness, which the previous methods cannot. The base of this method is to shed an electric arc on the base surface to be roughened. This arc works on melting and solidifying the base quickly; therefore, an unorganized surface is obtained. The operation is done by shedding the voltage difference on the base, which is bonded to one of the electrodes, and the second part is the copper wire brush that moves quickly on the base surface. So, this operation produces surfaces with roughness and bulges of molten metal (Picas *et al.* 2013). The Grit Blasted Method is adopted to roughen the research samples due to its availability, ease, and low cost.

5. Bond Coating of Preparation

This method is used to roughen the high hardness surfaces, which cannot be roughened by the traditional methods through which the thermal interactions are used to roughen the coating bases (Wielage *et al.* 2006).

2.7.2 Effect of spray parameters

The important steps which must be taken into consideration are to control the spray parameters to fit the purpose through which the coating process is implemented and include controllable parameters. They are spray angle distance in addition to the speed of drops. Also, changes occur during the spray process, which can be produced by oxidization, quick cooling, and other phenomena. The optimal choice is to take all the variables into consideration during the spray process (Hafiz Abd Malek *et al*. 2013, Hollis 2010, Fotovvati *et al.* 2019, Oliveira *et al.* 2020, Groza *et al.* 2007, Das 2007, Boulos *et al*. 2021).

1. Spray distance

It is the distance between the spray gun nozzle and the base where in the case of the near distance of spray, this may not give enough time for particles to melt, and at the same time, the oxidization of drops is decreased during the transfer. Also, the near distance of spray leads to overheating of the base and therefore obtaining a weak coating with irregular thickness. If the spray distance is far, the particles may be immobilized before reaching the target, resulting in increased porosity, reduced sedimentation efficiency, and drooping oxidation, which may affect coating properties such as hardness, porosity, and surface roughness of the coating.

2. Spray angle

The spray angle changes to fit with the base, and the porosity of the coating increases with the increase of the spray angle from (30º-60º). The level of porosity is not affected by the increase of angle until reaching the angle (90º), which is considered the best spray angle. The spray angle influences the adhesion of the coating layer.

3. Spray speed

The spray speed is considered one of the most critical parameters in thermal spray processes. It is preferred to spray the coating material at high speed to avoid a shift in the phase, especially when using carbon steel as the coating base. When using the slow speed, the temperature of the base is high compared with the high speeds. This means that spraying with low speed leads to heating the base, and therefore, we get a weak coating. Also, the high speeds give higher adhesion and decrease the porosity.

2.8 The Microstructure of Thermal Spray Coatings

The coating results from the repetitive sedimentation of particles with diameters of (10-120) mμ. The thermal spray coatings structure is lamellar and much like stacked cards, one on top of the other. Also, it is a complex structure that results from molten and semi-molten drops, and the metallic coatings include thin oxides resulting from the oxidization of particles during spray (Figure 2.14). Ceramic coatings always include cracks resulting from relaxation in the tensile process of coating (Lee *et al.* 2006, Rakesh *et al.* 2010).

The accurate structure of coating and the freezing of droops depend on the size of the droop, temperature, speed of drops, the distribution of nucleation parameters, and distance. In general, the nucleation of solid phases is either homogenous or inhomogeneous. It is tough to prevent inhomogeneous nucleation due to underlying nucleation factors. The microstructure is characterized by the closed porosities, cracks, and divisions of non-molten particles, and they generally affect the mechanical properties of the coating. In general, the heterogeneous composition reduces the hardness, tensile, and uniformity of the coating, and these thermally sprayed coatings are anisotropic, which further complicates the mechanical properties (Das 2007, Rybin *et al.* 2021).

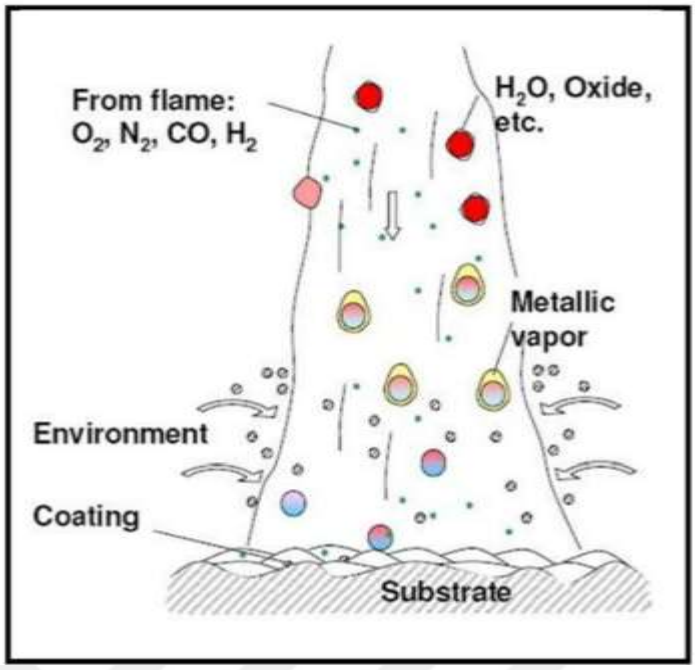

Figure 2.14 The spray process and coating structure (Das 2007)

2.9 The porosity of Thermal Spray Coatings

Porosities in the coating layer may result during different processes, and generally, there are three aggregates of porosities and can be summarized as follows (Sarikaya 2005).

1. Inter lamellar pores.
2. Spherical pores
3. Inter splat pores

Differences between the structure of pores are mainly produced for the smelting phase and the collision speed of particles. Porosities between layers are parallel with the typically coated base and formed because of the lack of cohesion between the divisions. In terms of spherical pores, they are formed due to the incomplete melting or quick freezing of particles. In contrast, cracks are formed because of the relaxation in the tensile of the system (base-coating) with the difference in the thermal diffusion coefficient (Tarasi *et al.* 2008). Porosity in precipitated layers influences many properties of the coating layer, such as the mechanical properties, including solidity,

tensile, and others, and physical properties such as thermal conductivity and electrical insulation of the coating layer. Evaluation of porosity size is the primary way to describe the microstructure of thermal spray through the density affected by the particle speed. It is found that density increased because of the high speed of particles which in turn gives high momentum for particles. This promotes overlapping related divisions, which enhance the final solidity of the coating. Porosity is also affected by the existence of oxides formed during the transfer of droops to the base. The oxidization process of transferred droops increases whenever the distance increases (Darut *et al.* 2021, Jadidi *et al*. 2015). The porosity of thermal spray can be classified according to the underlying formation mechanism, as shown in Figure 2.15 (Jung *et al.* 2016).

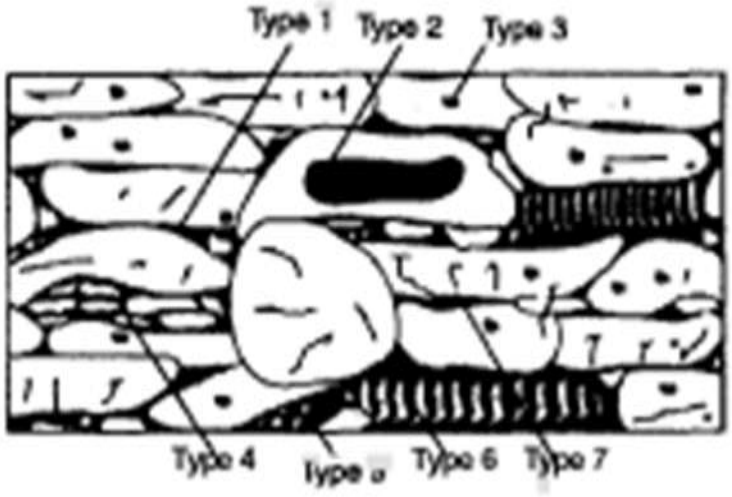

Figure 2.15 The porosity of thermal spray according to the underlying mechanism of particle distribution (Jung *et al*. 2016)

The first type (Type 1) is the porosity between the plates formed by stacking separated particles. This type of porosity is directly associated with the spray material's grit size and distribution properties. The second type (type 2) is classified according to the gas pockets formed through the gas flow disturbance during the spray process. The third type (type 3) of porosity is associated with the gas bubbles formed by the disintegration of the gas to the molten metal and released when freezing the metal. The fourth type (type 4) of porosity is formed because of particle atomization at the collision during the spray process. The fifth type (type 5) of porosity is formed from the partial condensation of vaporized particles which always include the residuals of powder.

The sixth type (type 6) results from shrinkage and freezing between the arms. The seventh type (type 7) of porosity results from cracks considered. In general, it is possible to decrease or eliminate pores by increasing the speed of particles or making the spray process under different pressures.

2.10 The Hardness of Thermal Spray Coatings

Hardness is one of the mechanical methods for material testing. The hardness is defined as the material's resistance to the plastic deformation; it is the indention resistance of a material or scratching resistance or crush. The material's resistance to penetration is generally considered the base to measure the hardness. The hardness techniques were developed with time through which it is possible to penetrate towards the surface for material exposed for testing under the control conditions of load and application ratio. The deep or size of resulted penetration can be measured, and the transformation is associated with the value of hardness, where the flexible material is offset by the deepest and largest penetration (Chandra *et al.* 2009).

Hardness measurement can be macro or micro based on the powder and obtained distances. It must be mentioned that the hardness property depends on the material's structure, the temperature, the type of medium dealt with, or the point of softness. The last property also depends on the bonding strength between atoms or molecules in the material. Whenever the bonding is more robust and atoms are associated, the value of hardness is increased. This means that the bodies fully by pores have less penetration resistance than those free of pores. The hardness of thermal spray coatings is significant as the case with wearing protective coatings. Generally, there are many hardness measurements as follows (Das 2007, Chandra *et al.* 2009):

1. Brinell hardness (BH).
2. No hardness (NH).
3. Vickers hardness (VH).

In the study project, Vickers hardness measurement is adopted, which depends on the application of specific power by diamond implant tool on the form of a pyramid with a quad base. The vertical angle amounted to 136 º between the two opposite sides, and the effect form performed by the penetration tool is on the form of rhombus through which the hardness of the metal is found (Figure 2.16).

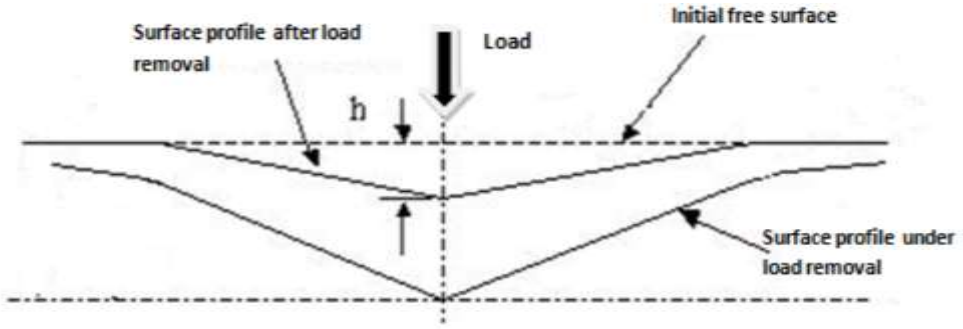

Figure 2.16 The shape of the effect conducted by the penetration tool on the metal surface (Chandra *et al.* 2009)

Values obtained by this test are suitable; therefore, this test gives logical values for hardness. Vickers hardness can be found by dividing the load on the actual area prone to compression.

2.11 Adhesion of Thermal Spray Coatings

Adhesion is the status where two surfaces adhere by forming interfacial strength between them. Also, the coating layer must characterize by the following (Pawlowski 2008, Tomaszek *et al.* 2007).

- It must firmly adhere to the base surface.
- They must be coherent with each other.
- It must be in the status of integration and continuity.
- It must be homogeneous in terms of thickness.

The adhesion process is necessary and is of the thermal spray coating conditions. The adhesion mechanisms to the bonding between the coating and base are characterized by three categories as follows (Das 2007). Physical interaction: It results from van der Waals forces, and the gap between the two surfaces is less than 0.5 nm to make Van der Waals force effective. Metallurgical interaction results through the diffusion or chemical interaction between the two surfaces. In Figure 2.17, mechanical interaction: it depends on the spray parameters related to the preparation of bases. The pressure affects the adhesion process because increasing the spray distance harms the adhesion process, and the collision of droops is more minor and therefore gives less adhesion in general. To get a thick coating with high bonding during the spray process, this needs a high velocity of particles that give a better coating (Das 2007).

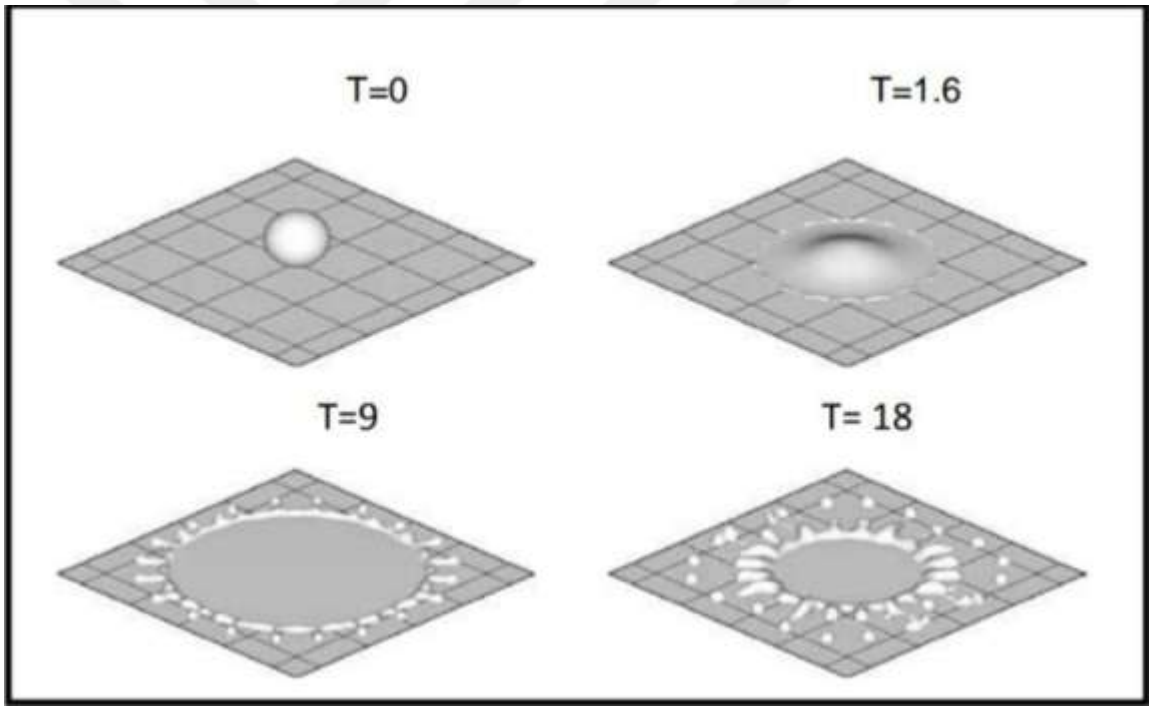

Figure 2.17 The shapes of droops at the collision

In Equation (2.2), T is the time parameter and is equal to

$$T = \frac{tv}{D} \tag{2.2}$$

D is the distance between the spray gun and the base, v is the velocity of particles, and t is the time consumed by the droops to reach the base or Time Fly.

3. MATERIALS AND METHODS

This chapter includes a review of the materials used in the production of spray material using the coating technique by the thermal spray technique. In addition, this chapter consists of the most critical laboratory tests conducted on the produced material, studying the effect of the spray process variable on the properties of these materials to evaluate the coating layer. The first part of this chapter reviews a description of the used materials and devices in coatings, the samples, and the technical diagram in the preparation and manufacturing of coating. The second part includes the laboratory tests.

3.1 Flame Spray System

The flame thermal spray system is shown in Figure 3.1, which explains the used spray gun type (GH - 4/h, China). It is made in China to spray the powder cermet towards the coating base (metal+ carped).

Figure 3.1 Flame thermal spray system

A unique holder has been designed which holds the spray gun and is installed at a distance that can be changed towards the load base of samples. The temperature necessary to melt the coating powder can be obtained by the combustion of fuel gaseous mixed with a specific oxygen ratio of about 4 bar and acetylene at 0.7 bar. At the same time, the selected materials (metal+ carped) are fed by a crucible placed on the top of the gun, and the opening and closing processes can be controlled during the spray process. When these materials reach the gas flame duct, these materials will be totally or partially molten. At the same time, the applied pressure will carry out the molten drops quickly to the prepared surface (the essential base). Also, the combustion pressure gases work intensely as a pumping power of molten particles and accelerate it up to (100 m/s) (Korotcenkov 2020). The following features characterize this spray gun:

- Lightweight, easy to carry, and controlled.
- High possibility of changing the direction and altitude.
- Easy to maintain.

3.2 Base for Holding Samples

A base was made to install the samples during the spray process, and its diameter was 20 cm. It has been perforated into eight holes, and the diameter of each hole is 2 cm. The base has been perforated from the top of each hole, and insert the screw to install the samples and prevent them from moving during the spray process. The circular base has been installed on the unique base, with an altitude of 50 cm, as shown below in Figure 3.2.

Figure 3.2 Samples installation base

3.3 Materials and Equipment Used in the Research

3.3.1 Aluminum coating material- tungsten carbide (Al-WC)

The nickel-metal (Al), produced by the German Riedel –De Haen AG seelze – Hannover Company, has been used with a granular size of about 90 µm and purity of 99.8%. Also, the tungsten carbide (WC) made by the Chinese Changsha Santech Materials Co., Ltd Company has been used with a granular size of 200 µm with a purity of 99.8%, and Figure 3.3 explains the used materials in the spray process.

Figure 3.3 The used materials in the spray process

3.3.2 Bond coating (Ni-Al)

A bond material manufactured by Metco Company with No. 65C and granular size (75-100 μm) has been used because of its good resistance against oxidization at high temperatures and its homogeneity with good adhesion strength between the substrates and coating layers. Figure 3.4 shows the used bonding material.

Figure 3.4 The used bonding material

3.3.3 Substrate of coating

A turbine plate manufactured by Siemens Company, clarified in Figure 3.5. and Table 3.1, has been used due to its high resistance to high temperatures reaching 3500° C.

Figure 3.5 The turbine plate before cutting

Table 3.1 The elements of the damaged turbine plate used in the current study

Elements	**The ratio%**
C	0.03<
Si	1.00<
Mn	2.00<
P	0.04≤
S	0.03≤
Cr	17.00
Mo	2.25
Ni	12.00
Fe	Remain

The plate has been cut into small pieces with a diameter of (1cm2) as shown in Figure 3.6 below.

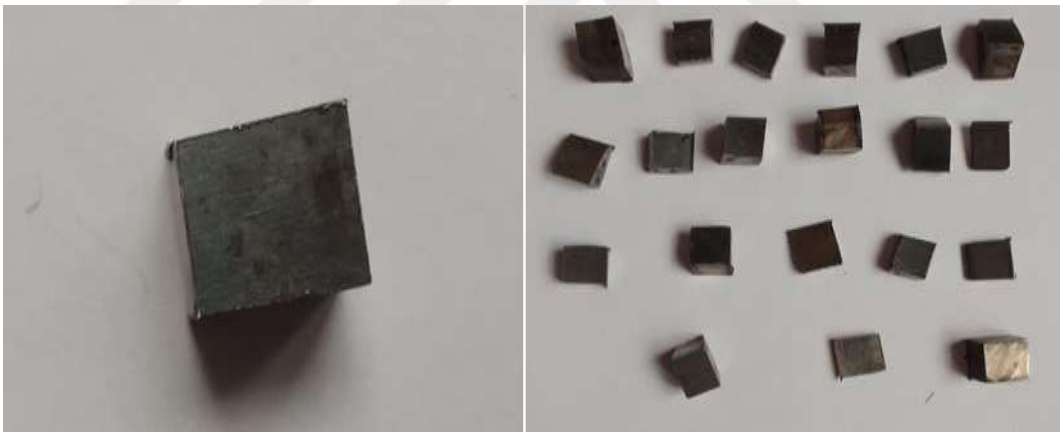

Figure 3.6 The turbine plate after cutting

3.4 Preparation of Samples

3.4.1 The Preparation of the coating material

The materials (Al + WC) were prepared by mixing the materials in an electric mixer with Teflon balls for 2 hr to get a homogeneous mixture. The materials were mixed based on the ratios shown in Table 3.2.

Table 3.2 The weights ratios of materials mixing (Al-%WC)

Number	WC%	AL%
1	5	95
2	10	90
3	15	85
4	20	80
5	25	75
6	30	70

Later, an initial treatment (annealing) was conducted on the materials at a temperature of 150°C for 1 hr using an American-made KSL 1200X oven. The purpose of thermal treatment before the coating process is to dry the particle of materials from the effect of humidity. Therefore, the particles will be in good elastic condition and qualified to produce coatings with good adhesive strength with the primary material.

3.4.2 Sample preparation for coating

After the cutting process, the samples were prepared before the coating process, where the preparation process is considered one of the most important means for the success of the coating process. The preparation process has been implemented in many stages, where the roughening process is implemented by the bond coating of the base surface. Then, it was washed with distilled water and soap, and then it was washed with ethanol alcohol to remove the suspended fatty materials and get a suitable surface to perform the coating process. The surface preparation and coating period must be done as fast as possible and confirmed not to catch the samples from the surface by hand. Regarding porosity samples and X-ray checking, we do not use the roughen process where we only use the cleaning process to separate the samples from bases and examine them. It is necessary to mention that the initial coating process has been done by Ni–Al before the primary coating to increase the adhesion strength of the coating material with the base. Figure 3.7 is represents a model from the samples.

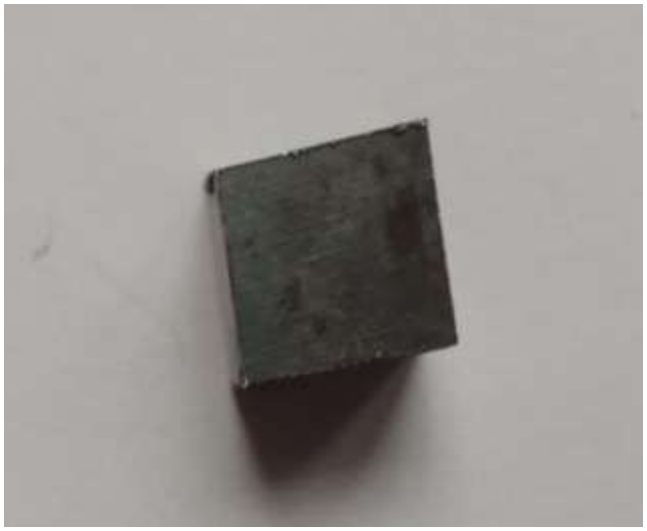

Figure 3.7 Represents model from the samples

3.5 The Coating Process

The coating process on prepared samples has been done using the thermal spray process by flame method, which has been used to coat all the prepared samples in this study. Figure 3.8 is explains the flame spray system.

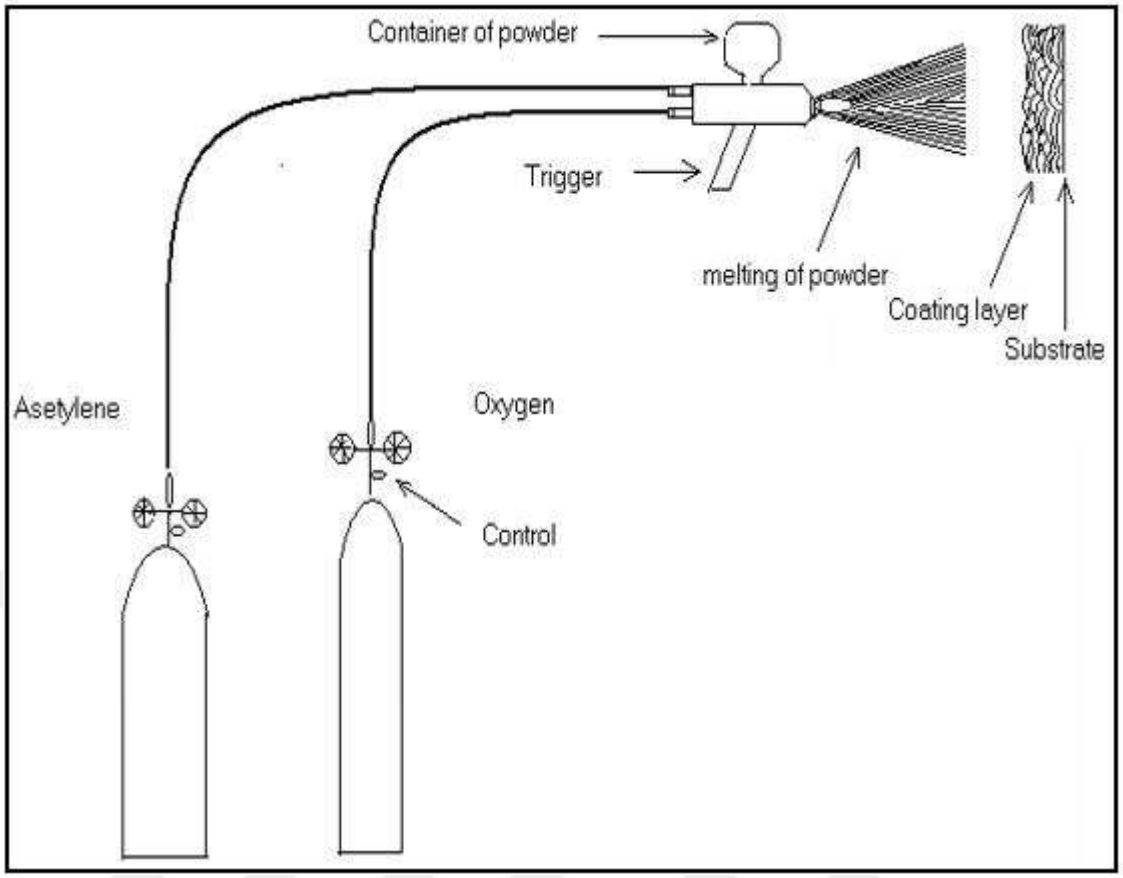

Figure 3.8 Flame spray system

The gas fuel combustion obtains the temperature required to melt the coating powder. The mixing ratio of oxygen with acetylene was determined. The best ratio was (4 bar) for oxygen and (0.7 bar) for acetylene through the unique regulator. At the same time, the power of the selected material they fed by a crucible placed at the top of the device, and the opening and closing process is controlled during the spray process. When the powders reach the gas flame duct, they will be entirely or partially melted while the pressure of gases loads the melted droops quickly towards the prepared surface (the essential base). In addition, the pressure of combustion gases works as a driving force to the melted particles and accelerates quickly with a speed reach to (100 m/sec). In Figure 3.9 explains the prepared models by the flame thermal spray method.

Figure 3.9 The prepared models by flame spray method

The spraying process was implemented from a distance of 15 cm, and the distance represents one of the spraying parameters while the spray angle was (90°). Table 3.3 explains spray process parameters obtained through the practical experiments.

Table 3.3 The spray process parameters

The mixing ration of oxygen and acetylene	0.7:4
The spray distance	15cm
The torch temperature	(3000-3300) °C
The granular size of the powder	(90-200) mμ
The coating thickness	1.45 mm

3.6 The Thermal Treatment

The thermal treatment has been implemented on the coating samples to get rid of pores that impair the properties of the coating. The thermal treatment was done in a standard atmosphere using an American electric oven of KSL 1200X. The samples were placed

at a temperature of 1000°C for 2 hr to get a stable internal structure. Based on prior studies, this point has been taken that the thermal treatment value above or under 1000°C gives undesired properties to the coating layers. Figure 3.10 explains the used electric oven in the metal treatments.

Figure 3.10 The electric oven used in thermal treatments

3.7 Physical and Mechanical Tests

3.7.1 Porosity test

The existence of pores in the thermal spray coatings is of the most distinctive properties of those coatings and effectively influences the coating properties. So, the porosity is measured through coatings layers that have been coated on a rough surface because of ease of separating from the base, and the concept of the Immersion Method of Archimedes is adopted to find the porosity according to American Standards for Testing

of Materials (ASTM) based on the property (ASTM-830) (Javaherdashti *et al.* 2016). This was based on the following steps:

1. Drying the samples for twenty minutes using the electric oven at a temperature of 75°C, the samples are weighted by a sensitive scale of type (Mettler) and accuracy of 0.0001.
2. The samples were immersed in a container full of distilled water for (24 hr) and weighed the samples immersed by water.
3. The samples were weighed when they were immersed and hung in the water.
4. The ratio of open pores can be calculated assuming that the dry weight is W1, saturated weight W2, and hang weight W3 according to the following mathematical Equation (3.1):

$$\text{Porosity} = \left(\frac{W_2 - W_1}{W_2 - W_3}\right) \times 100\% \qquad (3.1)$$

3.7.2 Hardness test

The hardness property is the resistance of surface material to the permanent deformation which occurs through the indentation, cut, wear, scratching, penetration and machinability. The hardness of material depends on the type of bonding strength between molecules or atoms, the type of surface, high temperature, and thermal parameters (Mohamed *et al.* 2008). The micro hardness test of type Vickers has been conducted by the hardness device of type METKON, of French origin, which includes the penetration tool and tapered microscopic head on the form of a square base diamond pyramid and its levels intersect at the top within an angle of 136°. The sample is installed under this tool; therefore, the samples were cut with a length of 1cm, a width of 1cm, and a thickness of 1cm, where it applied a load of 50N and timed 20sec. Vickers number of hardness is calculated by measuring the lengths of the two diameters (d1 and d2) and the average value to them (D) and then applying the following Equation (3.2):

$$HV = \frac{2f\sin\frac{136^\circ}{2}}{d_{av}} \qquad HV = 1.854\,\frac{f}{d_{av}} \tag{3.2}$$

Where:

HV: Vickers hardness.

f: the applied load (N).

d_{av} : average impact diameter.

The hardness in many regions of the sample was measured where the hardness on edges and center are taken and summed to obtain approximated value to the hardness average. (Figure 3.11) explains a photo of the hardness measure device of type (METKON), French origin, which exists in the University of Tikrit-College of Engineering-Mechanical Department.

Figure 3.11. Vickers device of hardness measure

3.7.3 Adhesion force inspect

The adhesion test of coating layers has been conducted by using the tensile strength device of type Microcomputer Controlled Electronic Universal Testing Machine (WDW-50E) with maximum load amounted (1.5 ton) and manufactured by the Germany company (Time Group Inc.) according to the properties (ASTM A370). Figure 3.12 explains the tensile test device in the Ministry of Science and Technology\ Department of Material Research.

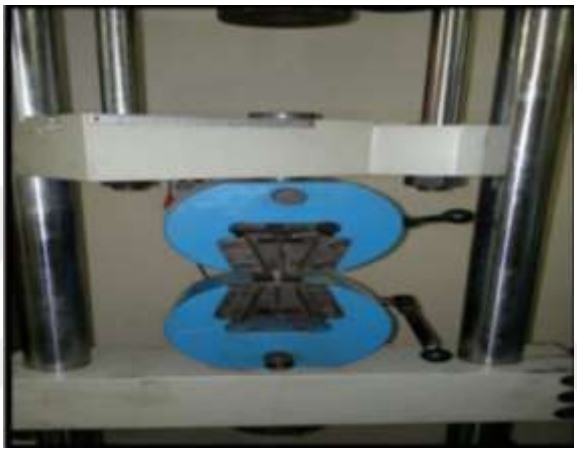

Figure 3.12 The tensile test device

The adhesion samples were installed in the jaws of tensile device as shown in Figure 3.13.

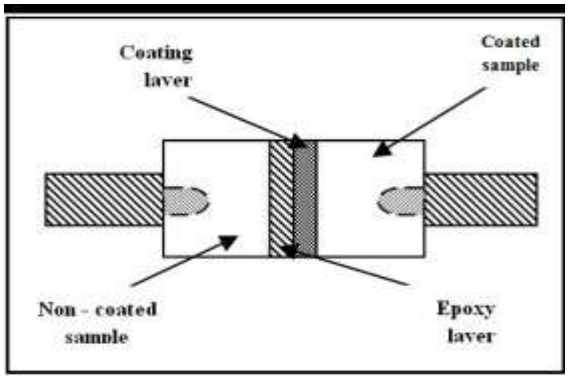

Figure 3.13 A method of installing the adhesion samples in the jaws of the tensile device

During the conduction of the adhesion test, the following methods were followed:

1. We are preparing samples of the base material without coating with an equal number of sprayed samples and exact measurement dimensions.
2. We are conducting the chemical cleaning by using alcohol on each sprayed and unsprayed sample to eliminate the pollutants that hinder the adhesion process of the two pieces.
3. Use adhesive epoxy to glue the two samples together (the sprayed and unsprayed) and then put a regular thin layer of the adhesive on the coating surface where all coating area is covered. Then the two pieces are pressed together for about two hours and put in a dried oven for 24 hr and at a temperature of 50°C. Before conducting the tensile experiment, it is necessary to consider the regularity of adhesion. When conducting the checking process, the applied tensile force must be on the surface exactly.
4. The tensile load has been applied for each sample with a tensile average of 1mm/min until a failure to the sample happens where the highest applied load is registered.
5. The following formula calculates the adhesion force or resistance of the coating material:

$$The\ adhesion\ force = \frac{The\ highest\ applied\ laod}{The\ area\ of\ sample\ surface} \tag{3.3}$$

3.7.4 X-Ray diffraction analysis

X-ray diffraction of the materials (metal + carped) has been measured using a device of type X'Pert High Score Plus, Dutch origin, which exists in Iran\ Kashan University. The used tube was (Cu) kα, and the examinations were at room temperature. Table 3.4 explains the properties of the x-ray diffraction device.

Table 3.4 The properties of x-ray diffraction device

Voltage	40 Kv
Current	30 Ma
Scan speed	5 deg⁄min
Scan speed	5° - 80°
Wavelength	1.54060 A°

We were provided the interval distance values of the atomic levels (d) for each concentration. The intervals are obtained by comparing the values of intercellular distances (d) with ray intensity and angle 2Θ based on standard tables related to used materials to obtain Miller's coefficients. Figure 3.14 explains the (XRD – 6000SHIMADZU) device used in the study.

Figure 3.14 System to check the x-ray diffraction

In order to calculate the curved width at the middle of greatest intensity ()β, we use the following formula:

$$\beta = \text{FWHM} \times \frac{2\pi}{360} \tag{3.4}$$

Where:

(β): The radian unit measures the package width at the middle of the most incredible intensity. The average grit size for any crystalline materials is calculated by the use of Scherer's Formula as follows in Equation (3.5):

$$C.S = \frac{0.9\,\lambda}{\beta\,\cos\theta} \tag{3.5}$$

Where:

C.S: The average of grit size (nm).
λ: The wavelength of the incident X-ray.
(β): The curved width at the middle of the intensity.
θ: The diffraction angle at the middle of the intensity.

3.7.5 Scanning electron microscope test

The sample examinations were conducted in Iran- the University of Tehran using the Scanning Electron Microscope (SEM) of type (TESCAN) and model of MIRA3, French origin, as shown in Figure 3.15. The electron microscope is characterized more than other optical microscopes by using electrons instead of optical waves, which give detailed enlarged three-dimensional images. The image is black and white because it does not depend on optical waves, and samples to be checked are put inside the column deflated by an inlet or an airtight stopped. The device samples are silver or gold plated to have conductivity because the microscope illuminates the samples by shedding the electrons on them after deflating air. The electronic cannon launches a high-energy beam of electrons towards a series of magnetic lenses designed to collect that package in a precise location near the deflated column. A set of magnetic scanning files moves

the focused beam of electrons above the sample to be checked back and forth where the whole sample is covered. When touching the electronic beam of the sample surface, some secondary electrons move from the sample surface, and the liberated electrons are detected across the special detector. The final image is formed based on the number of liberated electrons from each point of the sample surface. Thus, the resulting image will simulate and be compatible with the sample (De Biasi *et al.* 2019).

Figure 3.15 The scanning electronic microscope (SEM) system

4. RESULTS AND DISCUSSION

This chapter displays the analyses and discussion of results that have been obtained by the examinations conducted on samples used in this study which were prepared by the thermal flame spray from (Al-%WC). The effect of weight ratio changes on the properties of the coating surface prepared by the spray method, represented by the surface topography using a Scanning Electron Microscope, and its effect on each of the porosity, hardness, and adhesion force were noticed. The review and discussion of results are performed after conducting the thermal coefficients of samples with a temperature of (1000°C). Also, this chapter displayed and analyzed the x-ray diffraction of the coating layer after spraying and conducting the thermal coefficients to note the phase changes and their effect on the coating properties.

Table 4.1 The results of Vickers hardness of coating (Ni-%WC)

S	Material	Hardness before sintering	Hardness after sintering
1	(95%Al-5%WC)	112	120
2	(90%Al-10%WC)	132	134
3	(85%Al-15%WC)	139	156
4	(80%Al-20%WC)	153	178
5	(75%Al-25%WC)	140	109

We see Table 4.1, which explains the relationship between the Tungsten Carbide ratio and hardness before sintering by 1000°C. We find that hardness starts with a gradual increase with the additional percentage of WC% (Figure 4.1). This refers to the clear and practical effect of the Tungsten Carbide on the primary material of aluminum Al until reaching the highest hardness ratio with a reinforcement ratio of 25% and hardness of 153 Hv. Later, it starts to reduce, and this is because the agglomeration resulting from reinforced material negatively works on the hardness, which hinders the mechanical interlocking process between the atoms for both the reinforcement and basic materials (Ross 2013).

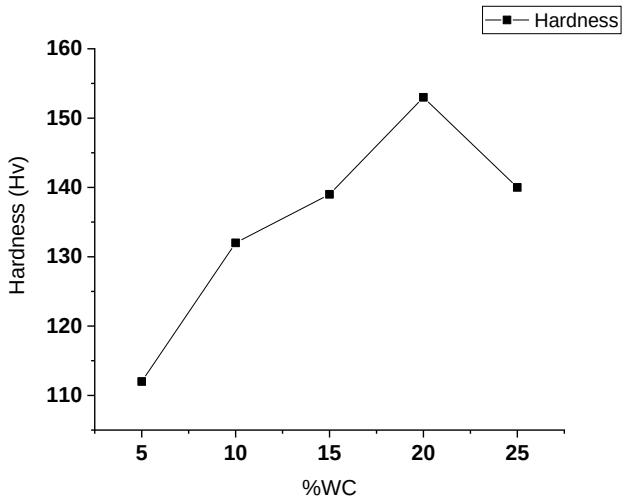

Figure 4.1 The hardness before sintering

While after sintering by 1000°, we find a high increase in the hardness with the addition ratios and reach 25% WC with a hardness of 178 (Figure 4.2, Figure 4.3). The main reason for this is that the thermal amount helps in the bonding and cohesion of atoms and increases the fusion power, reducing the porosity and the hardness. However, the hardness decrease after this percentage because of agglomeration of Tungsten Carbide WC (Suryanarayana and Grant 1998).

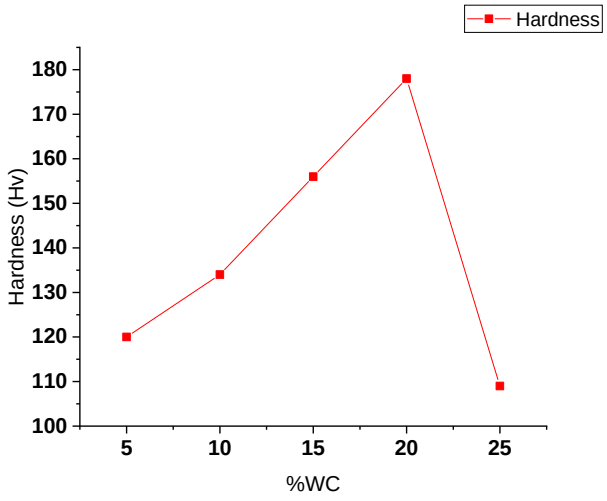

Figure 4.2 The hardness after sintering

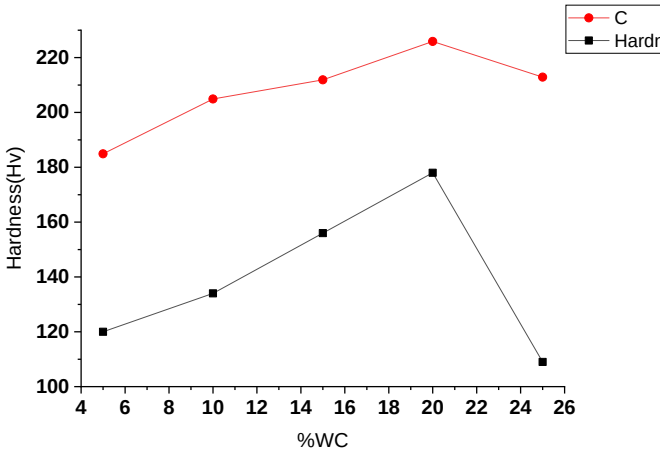

Figure 4.3 The relationship between Tungsten Carbide and hardness before and after the sintering

Table 4.2 explains the porosity values by the addition of Tungsten Carbide before and after the sintering.

Table 4.2 The porosity results of coating

S	Material	Hardness before sintering	Hardness after sintering
1	(95%Al-5%WC)	20	29
2	(90%Al-10%WC)	17	26
3	(85%Al-15%WC)	12	21
4	(80%Al-20%WC)	7	18
5	(75%Al-25%WC)	16	22

The porosity of the coating is considered one of the essential measures, which in turn gives a clear indicator of the strength and hardness of the coating. So, we can see from Figure 4.4 explain the relationship between the added Tungsten Carbide ratios and the porosity of coating before and after the thermal sintering by 1000°C. We see a high association between porosity and hardness. By increasing the reinforced period ratio of Tungsten Carbide, the percentage of porosity decreases until reaching a sintering value of 25% of the reinforcement material and is 18%. Figure 4.5 explains the porosity before sintering.

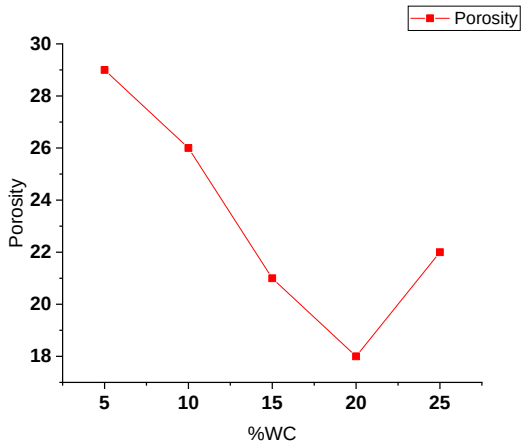

Figure 4.4 The porosity before sintering

While after sintering, the porosity decreased to 70% and at the same reinforcement ratio of 25% , all of this is due to the hardness, which means that porosity after sintering is lessened because the distance between atoms is reduced more than the case before sintering which is raised because of the difference of used materials in the coating and also the freezing of droops before reaching to the coating base (Ahmed 2012).

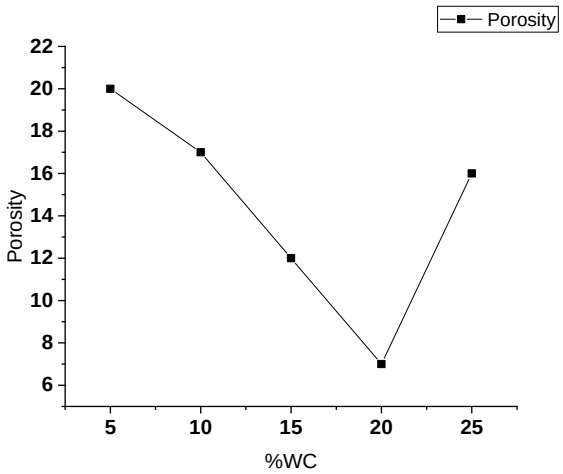

Figure 4.5 The porosity after sintering

Figure 4.6 and Table 4.3 explains the relationship between the Tungsten Carbide ratio and porosity before and after sintering.

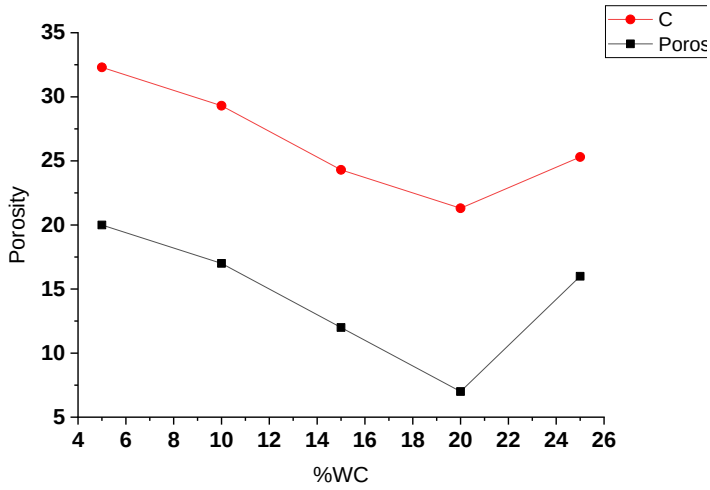

Figure 4.6 The porosity before and after sintering

Table 4.3 The adhesion force values before and after sintering

S	Material	Hardness before sintering	Hardness after sintering
1	(95%Al-5%WC)	18	11
2	(90%Al-10%WC)	24	15
3	(85%Al-15%WC)	28	18
4	(80%Al-20%WC)	33	23
5	(75%Al-25%WC)	25	19

The adhesion force is checking of coating, which results after the thermal spray has been conducted as a measure of the adhesion force of coating with the base, which in turn is considered a mechanical measure of the strength of coating between the reinforced material and basic. So, we can see from Figures (Figure 4.7, Figure 4.8, Figure 4.9), that the relationship between the adhesion force and the added Tungsten Carbide is from 5-30% before and after coating. Also, adding the added material increases the adhesion force between the base and coating until the highest adhesion force is obtained after the sintering. It is 33MPa with a reinforcement ratio of 25%, and later the adhesion force weakens. The reason behind this is that increasing the Carbide ratios will lead to the non-melting of the powder, ultimately which lead to the emergence of agglomeration inside the coating. The bonding between the coated materials is weakening, which happens in hardness and porosity where the distance between the thermal spray gun and the coating base has a high role in the increase and

decrease of the adhesion force and increasing the space leads to freezing the droops. Then the droops arrive molten to the coating base and cause the weakness of the adhesion force (Ahmed 2012).

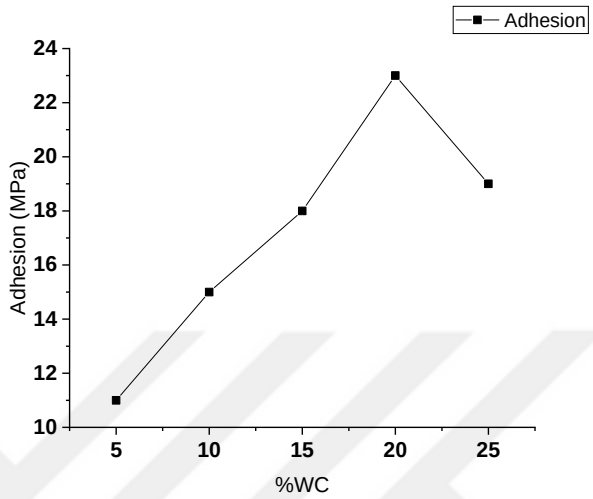

Figure 4.7 The adhesion force before sintering

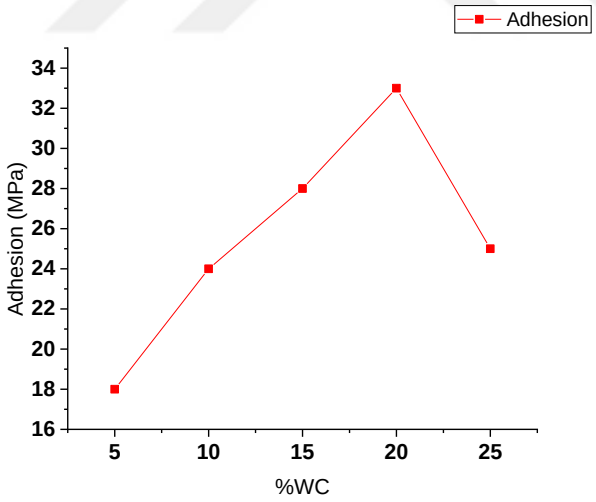

Figure 4.8 The adhesion force after the sintering

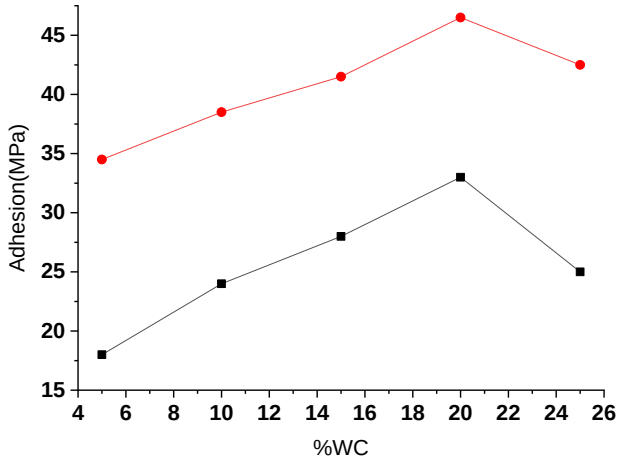

Figure 4.9 A comparison between the adhesion force before and after sintering

The crystal structure of the materials coated by the x-ray diffraction was identified where the x-ray diffraction found the surface analysis to know the phases formed on the sample's surfaces. This technique is considered one of the most important means to identify the nature and composition of the material used in the thermal spray process and control the phase changes on it. In Table 4.4 the crystal structure and phase change of the basic coating material and reinforced material of different ratios (5,10,15,20,25,30) were studied after conducting the spray process and thermally treated. Figure 4.10 explains the x-ray diffraction of the (%WC – Al) powder at the ratios, whereas Figure 4.11 shows the emergence of aluminum and Tungsten Carbide materials by comparing with ASTM. An increase in the crystal growth is noticed with slight displacements because of adding Tungsten Carbide and thermal treatment at 1000°C. Both affect the average crystal size, affecting the distances between crystal levels. Therefore it displaces the peak locations within the diffraction curve on the axis (2θ) into smaller or bigger values.

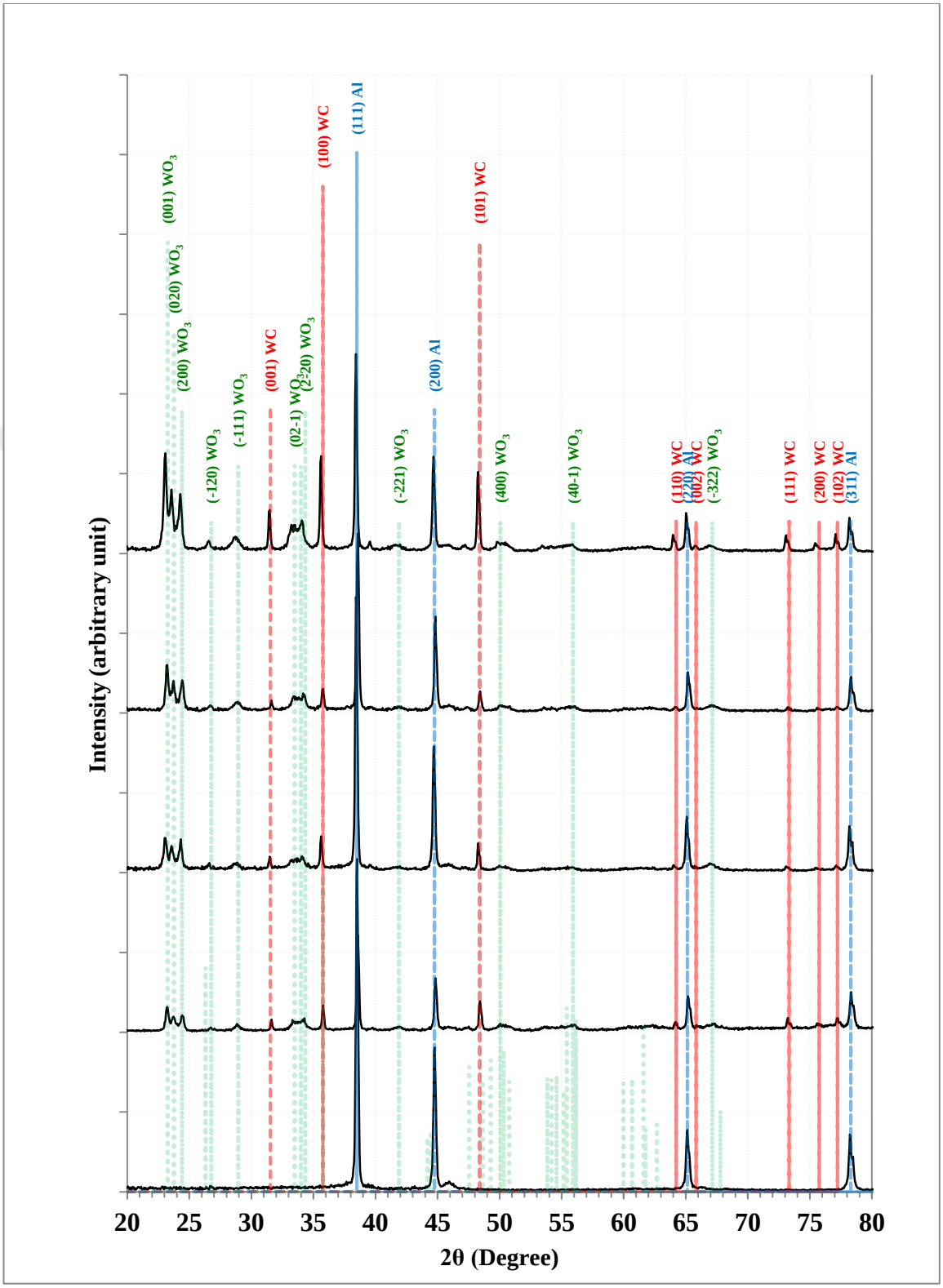

Figure 4.10 The x-ray diffraction results at different Tungsten Carbide ratio

Table 4.4 Results of checking the x-ray diffraction of the prepared coating at the ratios

WC (%)	2θ (Deg.)	FWHM (Deg.)	d_{hkl} Exp.(Å)	C.S (nm)	Phase	hkl	card No.
	38.5090	0.2776	2.3359	30.3	Cubic Al	(111)	96-431-3215
A	44.7712	0.2776	2.0226	31.0	Cubic Al	(200)	96-431-3215
	65.1311	0.3702	1.4311	25.5	Cubic Al	(220)	96-431-3215
	78.2416	0.4319	1.2208	23.7	Cubic Al	(311)	96-431-3215
	23.2082	0.2777	3.8295	29.2	Triclinic WO_3	(001)	96-101-0619
	23.7018	0.2776	3.7509	29.2	Triclinic WO_3	(020)	96-101-0619
	24.4113	0.3085	3.6434	26.3	Triclinic WO_3	(200)	96-101-0619
	26.7249	0.2468	3.3330	33.1	Triclinic WO_3	(-120)	96-101-0619
	28.8226	0.1851	3.0951	44.3	Triclinic WO_3	(-111)	96-101-0619
	31.6298	0.1851	2.8265	44.6	Cubic WC	(001)	96-150-1582
	33.3573	0.2468	2.6839	33.6	Triclinic WO_3	(02-1)	96-101-0619
B	34.2828	0.1851	2.6136	44.9	Triclinic WO_3	(2-20)	96-101-0619
	35.7943	0.2159	2.5066	38.7	Cubic WC	(100)	96-150-1582
	38.6015	0.2776	2.3305	30.3	Cubic Al	(111)	96-431-3215
	44.8329	0.2776	2.0200	31.0	Cubic Al	(200)	96-431-3215
	48.4113	0.2776	1.8787	31.4	Cubic WC	(101)	96-150-1582
	64.1748	0.2468	1.4501	38.0	Cubic WC	(110)	96-150-1582
	65.1928	0.4010	1.4299	23.5	Cubic Al	(220)	96-431-3215
	73.2134	0.2160	1.2918	45.8	Cubic WC	(111)	96-150-1582
	77.2545	0.2468	1.2340	41.2	Cubic WC	(102)	96-150-1582
	78.3342	0.4319	1.2196	23.7	Cubic Al	(311)	96-431-3215
	23.0231	0.3394	3.8599	23.9	Triclinic WO_3	(001)	96-101-0619
	23.5784	0.3084	3.7702	26.3	Triclinic WO_3	(020)	96-101-0619
	24.3188	0.3085	3.6571	26.3	Triclinic WO_3	(200)	96-101-0619
	26.6015	0.3085	3.3482	26.5	Triclinic WO_3	(-120)	96-101-0619
	28.8843	0.4319	3.0886	19.0	Triclinic WO_3	(-111)	96-101-0619
	31.4756	0.1851	2.8400	44.6	Cubic WC	(001)	96-150-1582
	33.3882	0.5862	2.6815	14.1	Triclinic WO_3	(02-1)	96-101-0619
C	34.0360	0.4319	2.6320	19.2	Triclinic WO_3	(2-20)	96-101-0619
	35.6093	0.2159	2.5192	38.6	Cubic WC	(100)	96-150-1582
	38.4165	0.2467	2.3413	34.1	Cubic Al	(111)	96-431-3215
	44.7095	0.2777	2.0253	30.9	Cubic Al	(200)	96-431-3215
	48.2879	0.2468	1.8832	35.3	Cubic WC	(101)	96-150-1582
	64.0206	0.1542	1.4532	60.8	Cubic WC	(110)	96-150-1582
	65.0694	0.3393	1.4323	27.8	Cubic Al	(220)	96-431-3215
	73.1208	0.2468	1.2932	40.1	Cubic WC	(111)	96-150-1582
	77.1003	0.2468	1.2360	41.2	Cubic WC	(102)	96-150-1582
	78.2108	0.3702	1.2212	27.7	Cubic Al	(311)	96-431-3215
	23.2082	0.3085	3.8295	26.3	Triclinic WO_3	(001)	96-101-0619
	23.7018	0.2467	3.7509	32.9	Triclinic WO_3	(020)	96-101-0619
	24.4113	0.3393	3.6434	24.0	Triclinic WO_3	(200)	96-101-0619

Table 4.4 (Continued)

	26.6941	0.3085	3.3368	26.5	Triclinic WO_3	(-120)	96-101-0619
	28.9152	0.4936	3.0854	16.6	Triclinic WO_3	(-111)	96-101-0619
	31.5990	0.2159	2.8292	38.2	Cubic WC	(001)	96-150-1582
	33.4190	0.4319	2.6791	19.2	Triclinic WO_3	(02-1)	96-101-0619
D	34.1594	0.4319	2.6227	19.2	Triclinic WO_3	(2-20)	96-101-0619
	35.7943	0.2468	2.5066	33.8	Cubic WC	(100)	96-150-1582
	38.5707	0.2468	2.3323	34.1	Cubic Al	(111)	96-431-3215
	44.8329	0.2776	2.0200	31.0	Cubic Al	(200)	96-431-3215
	48.4113	0.2776	1.8787	31.4	Cubic WC	(101)	96-150-1582
	64.1748	0.3393	1.4501	27.6	Cubic WC	(110)	96-150-1582
	65.1928	0.3085	1.4299	30.6	Cubic Al	(220)	96-431-3215
	73.2134	0.2160	1.2918	45.8	Cubic WC	(111)	96-150-1582
	77.2237	0.2467	1.2344	41.2	Cubic WC	(102)	96-150-1582
	78.3033	0.3702	1.2200	27.7	Cubic Al	(311)	96-431-3215
	23.0540	0.3085	3.8548	26.3	Triclinic WO_3	(001)	96-101-0619
	23.6093	0.3084	3.7654	26.3	Triclinic WO_3	(020)	96-101-0619
	24.2879	0.2776	3.6617	29.3	Triclinic WO_3	(200)	96-101-0619
	26.5707	0.3701	3.3520	22.1	Triclinic WO_3	(-120)	96-101-0619
	28.6684	0.6787	3.1114	12.1	Triclinic WO_3	(-111)	96-101-0619
	31.4139	0.2468	2.8454	33.4	Cubic WC	(001)	96-150-1582
	33.2031	0.4628	2.6960	17.9	Triclinic WO_3	(02-1)	96-101-0619
E	34.0668	0.4318	2.6296	19.2	Triclinic WO_3	(2-20)	96-101-0619
	35.6093	0.2159	2.5192	38.6	Cubic WC	(100)	96-150-1582
	38.4165	0.1850	2.3413	45.5	Cubic Al	(111)	96-431-3215
	44.6787	0.2468	2.0266	34.8	Cubic Al	(200)	96-431-3215
	48.2571	0.2468	1.8844	35.3	Cubic WC	(101)	96-150-1582
	49.8920	0.6479	1.8264	13.5	Triclinic WO_3	(400)	96-101-0619
	55.8458	0.4318	1.6449	20.8	Triclinic WO_3	(40-1)	96-101-0619
	63.9897	0.3085	1.4538	30.4	Cubic WC	(110)	96-150-1582
	65.0694	0.3702	1.4323	25.5	Cubic Al	(220)	96-431-3215
	65.7789	0.2777	1.4185	34.1	Cubic WC	(002)	96-150-1582
	73.0900	0.2159	1.2936	45.8	Cubic WC	(111)	96-150-1582
	75.4653	0.2776	1.2587	36.2	Cubic WC	(200)	96-150-1582
	77.1003	0.2160	1.2360	47.0	Cubic WC	(102)	96-150-1582
	78.1799	0.4319	1.2217	23.7	Cubic Al	(311)	96-431-3215

The surface topography of the samples sprayed by the thermal flame spray was studied. Figure 4.11 explains the scanning electron microscope with a depth of (10μm) and enlargement (5.00KX) to the samples model after conducting the thermal sintering at 1000°C with different reinforcement ratios of Tungsten Carbide. Image (a) explains the

reinforcement ratio of 5%, and we can realize the success of the coating process, but there is a randomness in distributing the nickel atoms during the surface of the sample; image (b) clearly explains the existence of reinforcement material spread through the nickel with very few quantities, randomness on the surface with reinforcement of 10% while the reinforcement ratio in the image (c) is 15% and we can find that it is a beginning to the surface regularity with apparent homogeneity and dimension between the nickel and Tungsten Carbide. In image (d) and with a reinforcement ratio of 20% of the Tungsten Carbide, we find the beginning of the crystal growth because of the temperature and apparent homogeneity between components. In comparison, we realize that an apparent and consistent surface was obtained in the image (d) with a 25% reinforcement ratio.

There is a distinctive crystal tangle between each base and reinforcement material with Tungsten Carbide distribution with all the surface components. This is consistent with the hardness, porosity, and adhesion force results. Whereas the image (e) gives a reinforcement ratio of 30%, we can find that there is randomness and irregularity compared with the model (e). So, we can find that the surface consistency and metallic interlocking between the coated material components have a high effect on the components of the coated material and highly increase the physical and mechanical properties (McMullan 1995).

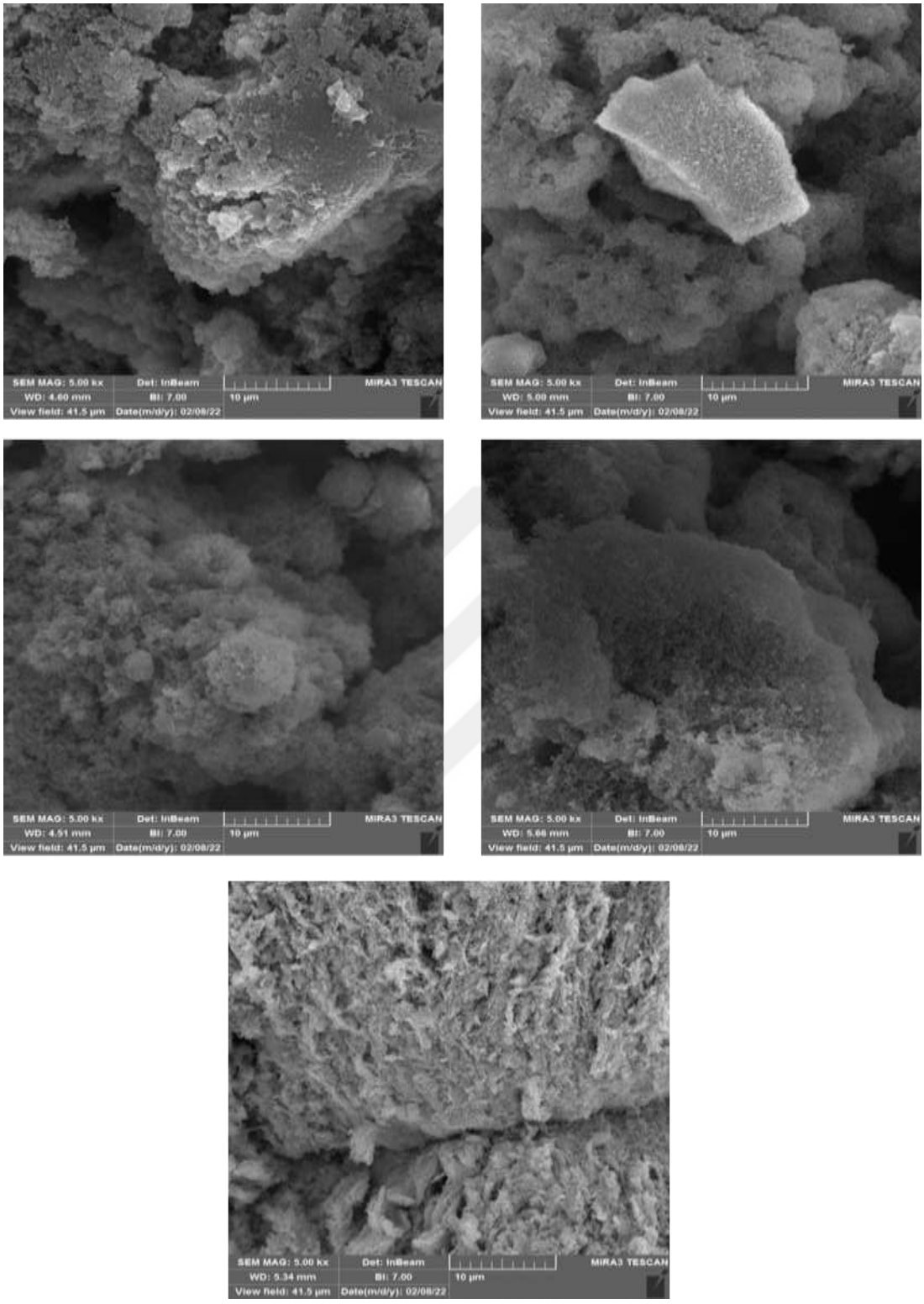

Figure 4.11 The scanning electron microscope to the model of samples at different reinforcement ratios and after the thermal sintering

5. CONCLUSIONS AND RECOMMENDATION

In this study, these conclusions were obtained in addition to the proposals for future projects in the current field by flame thermal spraying to treat turbine plates and oil pipe cracks. The following results were obtained

1. The best hardness value (153 HV) and the most negligible value of porosity (18%) were obtained at the spray distance of 15cm before the thermal treatment.
2. The best hardness value (178 HV) and the most negligible value of porosity (7%) were obtained after conducting the thermal treatment of (1000°C).
3. The best adhesion value of (23MPa) was obtained at a spray distance of 15cm before conducting the thermal treatment, and also we see that when conducting the thermal treatment of (1000 °C), we see that the adhesion force is increased (33MPa).
4. The relationship between porosity and hardness is inverse to the coating layers, where decreasing the porosity value increases the hardness value.
5. The process of obtaining the best hardness, porosity, and adhesion values was by adding 25% of Tungsten Carbide.
6. The effect of adding the Tungsten Carbide on the coating topography and with a reinforcement ratio of 25%, a very clear and regular surface was obtained, and there is a distinctive crystal tangle between each of the base material and reinforcement material with distribution to the Tungsten Carbide to all the surface parts. This is consistent with hardness, porosity, and adhesion force results.
7. The x-ray diffraction results show that the emergence of new phases and these phases increase the adhesion force and high hardness; therefore, the porosity is decreased.
8. The results of x-ray diffraction have proven the identity of the material which means the emergence of aluminum and Tungsten Carbide.
9. The emergence of such types of phases is because of adding specific ratios of Tungsten Carbide with a variable average (0,5,10,15,20,25) % and because the temperature generated from the spray device reaches (3500 °C).

Recommendation

1. Coating by using plasma spray process at the same spray distance of 15cm and spray angle of 90˚ and at the same weighting ratios and then compare the results between the two techniques.
2. Studying the effect of spray angles on the coating layer's properties and the spray distance and thermal treatment.
3. Using bases with different forms and studying the adhesion force.
4. Studying the properties of electrical insulation, thermal conductivity, and electrical resistance of the coating layers produced by the thermal spray.
5. Studying the properties of sintering and mechanical erosion to the coated materials.

REFERENCES

Abkenar, A. P. 2007. Wire-arc spraying system: particle production, transport, and deposition. Doctoral dissertation, University of Toronto, 133 page, Canada.

Ahmed, H. H. 2012. Fabrication and Study Characteristics Of CdS/Si Heterojunction Detector by CBD Technique. Tikrit Journal of Pure Science, 17(2): 3-7.

Ahmed, H. H., Ahmed, A. R., Darweesh, S. Y., Khodair, Z. T. and Al-Jubbori, M. A. 2020. Processing of Turbine Blades Using Cermet Composite Materials. Journal of Failure Analysis and Prevention, 20(6): 2111-2118.

Allen, R. C., Black, W. J. and McFarland, J. A. 2019. Development and diagnosis of an atmospheric pressure plasma torch for investigating magnetohydrodynamic instabilities. Journal of Physics D: Applied Physics, 52(17): 175-201.

Al-Shehri, Y. A. 2011. Mechanical and metallurgical properties of two-layered diamalloy 4010 and 2002 HVOF coating. Doctoral dissertation, Dublin City University, 136 page, Ireland.

Al-Taha, Z. Y. 2009. Investigation into laser re-melting of Inconel 625 HVOF coating blended with WC. Doctoral dissertation, Dublin City University, 152 page, Ireland.

Anupam, A., Kottada, R. S., Kashyap, S., Meghwal, A., Murty, B. S., Berndt, C. C. and Ang, A. S. M. 2020. Understanding the microstructural evolution of high entropy alloy coatings manufactured by atmospheric plasma spray processing. Applied Surface Science, 505: 117-144.

Avner, S. H. 1974. Introduction to physical metallurgy (Vol. 2). McGraw-hill, pp. 481-497, New York.

Bai, C. Y., Luo, Y. J. and Koo, C. H. 2004. Improvement of high temperature oxidation and corrosion resistance of superalloy IN-738LC by pack cementation. Surface and Coatings Technology, 183(1): 74-88.

Ballard, W. E. 1966. Metal spraying and the flame deposition of ceramics and plastics. Charles Griffen and Co Ltd, 591 page, London.

Beg, A. 2020. Comparison Of Mechanical Properties And Heat Affected Zone Of 304stainless Steel Of Joints By Tig Welding And Electric Arc Welding. MSc. Thesis, Integral University, 126 page, India.

Berndt, C. C., Khor, K. A. and Lugscheider, E. F. 2001. Thermal Spray 2001: New Surfaces for a New Millenium; Proceedings of the 2nd International Thermal Spray Conference. ASM International, 1410 page, Singapore.

Boulos, M. I., Fauchais, P. L. and Heberlein, J. V. 2021. Combustion Spraying. In Thermal Spray Fundamentals. Springer, pp. 235-302, USA.

Chaithanya, M. 2007. processing & characterization of nickel–aluminide coating on metal substrates. MSc. Thesis, National Institute of Technology Rourkela, 80 page, India.

Chandra, S. and Fauchais, P. 2009. Formation of solid splats during thermal spray deposition. Journal of Thermal Spray Technology, 18(2): 148-180.

Darut, G., Dieu, S., Schnuriger, B., Vignes, A., Morgeneyer, M., Lezzier, F. and Le Bihan, O. 2021. State of the art of particle emissions in thermal spraying and other high energy processes based on metal powders. Journal of Cleaner Production, 303: 5-13.

Darweesh, S. Y., Ali, A. M., Khodair, Z. T. and Majeed, Z. N. 2019. The effect of some physical and mechanical properties of cermet coating on petroleum pipes prepared by thermal spray method. Journal of Failure Analysis and Prevention, 19(6): 1726-1738.

Das, S. 2007. Study of Plasma Spray Alumina-Aluminide Composite Coating on Metals. Doctoral dissertation, National Institute of Technology Rourkela, 128 page, India.

Davis, J. R. 2001. Surface engineering for corrosion and wear resistance. ASM international, 288 page, USA.

De Biasi, L., Schwarz, B., Brezesinski, T., Hartmann, P., Janek, J. and Ehrenberg, H. 2019. Chemical, structural, and electronic aspects of formation and degradation behavior on different length scales of Ni- rich NCM and Li- rich HE- NCM cathode materials in Li- ion batteries. Advanced Materials, 31(26): 7-12.

De Silva, M. B. 2010. Study of microstructure effect on the thermal properties of Yttria-stabilized-Zirconia thermal barrier coatings made by atmospheric plasma spray

and pressing machine. Doctoral dissertation, University of Zulia, 97 page, Venezuela.

Dorfman, M. R. 2002. Thermal spray basics. Advanced materials and processes, 160(7): 47-51.

Fotovvati, B., Namdari, N. and Dehghanghadikolaei, A. 2019. On coating techniques for surface protection: A review. Journal of Manufacturing and Materials processing, 3(1): 19-28.

Gerdeman, D. A. and Hecht, N. L. 2012. Arc plasma technology in materials science. Springer Science and Business Media, 206 page, New York.

Grewal, H. S., Singh, H. and Agrawal, A. 2013. Microstructural and mechanical characterization of thermal sprayed nickel–alumina composite coatings. Surface and coatings Technology, 216: 78-92.

Groza, J. R. and Shackelford, J. F. 2007. Materials processing handbook. CRC press, 840 page, New York.

Hafiz Abd Malek, M., Hayati Saad, N., Kiyai Abas, S. and Mohd Shah, N. 2013. Thermal arc spray overview. In Materials Science and Engineering Conference Series, 46: 12-28.

Heimann, R. B. 2008. Plasma-spray coating: principles and applications. John Wiley and Sons, 354 page, USA.

Hollis, K. J. 2010. Zirconium diffusion barrier coatings for uranium fuel used in nuclear reactors. Advanced Materials and Processes, 168: 2-7.

Holmes, D. R. and Rahmel, A. 1977. Materials and coatings to resist high temperature corrosion. Dusseldorf, West Germany, 2: 6-11.

Hotea, V., Smical, I., Pop, E., Juhasz, I. and Badescu, G. 2008. Thermal Spray Coatings for Modern Technological Applications. Fascicle of Management and Technological Engineering, 7: 1486-1492.

J Talib, R. J., Saad, S., Toff, M. R. M. and Hashim, H. 2003. Thermal spray coating technology: A review. Solid State Sci Technol, 11(1): 109-117.

Jadidi, M., Moghtadernejad, S. and Dolatabadi, A. 2015. A comprehensive review on fluid dynamics and transport of suspension/liquid droplets and particles in high-velocity oxygen-fuel (HVOF) thermal spray. Coatings, 5(4): 576-645.

Javaherdashti, R., Nwaoha, C. and Tan, H. 2016. Corrosion and materials in the oil and gas industries. CRC Press, 271 page, USA.

Jehn, H. A. 2000. Improvement of the corrosion resistance of PVD hard coating–substrate systems. Surface and Coatings Technology, 125(1-3): 212-217.

Jung, J., Jeong, S. and Kim, H. 2016. Investigation of single-droplet/wall collision heat transfer characteristics using infrared thermometry. International Journal of Heat and Mass Transfer, 92: 774-783.

Kawakita, J., Fukushima, T., Kuroda, S. and Kodama, T. 2002. Corrosion behaviour of HVOF sprayed SUS316L stainless steel in seawater. Corrosion science, 44(11): 2561-2581.

Korotcenkov, G. 2020. Metal Oxide Powder Technologies: Fundamentals, Processing Methods and Applications. Elsevier, 446 page, USA.

Kucuk, A., Lima, R. S. and Berndt, C. C. 2000. Composite coatings of Si3N4-soda lime silica produced by the thermal spray process. Journal of materials engineering and performance, 9(6): 603-608.

Łatka, L., Pawłowski, L., Winnicki, M., Sokołowski, P., Małachowska, A. and Kozerski, S. 2020. Review of functionally graded thermal sprayed coatings. Applied Sciences, 10(15): 5153.

Lee, H. S., Singh, J. K., Ismail, M. A., Bhattacharya, C., Seikh, A. H., Alharthi, N. and Hussain, R. R. 2019. Corrosion mechanism and kinetics of Al-Zn coating deposited by arc thermal spraying process in saline solution at prolong exposure periods. Scientific reports, 9(1): 1-17.

Lee, K., Park, J., Ye, K., Jeon, C., Kim, S., Song, Y. and Lee, D. Y. 2006. Acoustic emission source analysis of vacuum plasma sprayed CoNiCrAlY coatings. journal-korean physical society, 48(6): 1691.

Li, C. J. and Ohmori, A. 2002. Relationships between the microstructure and properties of thermally sprayed deposits. Journal of thermal spray technology, 11(3): 365-374.

Li, M. and Christofides, P. D. 2003. Modeling and analysis of HVOF thermal spray process accounting for powder size distribution. Chemical Engineering Science, 58(3-6): 849-857.

Liu, S. H., Trelles, J. P., Murphy, A. B., He, W. T., Shi, J., Li, S., ... & Guo, H. B. 2021. Low-pressure plasma-induced physical vapor deposition of advanced thermal barrier coatings: Microstructures, modelling and mechanisms. Materials Today Physics, 21: 6-9.

Malek, M. H. A., Saad, N. H., Abas, S. K. and Shah, N. B. M. 2014. Critical process and performance parameters of thermal arc spray coating. International Journal of Materials Engineering Innovation, 5(1): 12-27.

Martengo, P.C. and Caruchi. 1987. Materials and coating to resist high temperature corrosion. CRC press, 223 page, UK.

Matthews, S., James, B. and Hyland, M. 2008. Erosion of oxide scales formed on Cr3C2–NiCr thermal spray coatings. Corrosion Science, 50(11): 3087-3094.

Mbaya, J. H., and Hannafi, J. 2021. Mathematical modeling of fluid flow and total heat transfer process in wellbore.Scince World Journal, 16(2): 133-137.

McMullan, D. 1995. Scanning electron microscopy 1928–1965. Scanning, 17(3): 175-185.

Meetham, G. W. and Van de Voorde, M. H. 2000. Materials for high temperature engineering applications. Springer Science and Business Media, 164 psge, New York.

Mohamed, H. A. H. and Ali, H. M. 2008. Characterization of ITO/CdO/glass thin films evaporated by electron beam technique. Science and technology of advanced materials, 9(2): 5016 -5025.

Mondolfo, L. F. 1985a. Aluminum Alloys : structure and properties. Elsevier, 982 psge, London .

Mondolfo, L. F. 2013b. Aluminum alloys: structure and properties. Elsevier, 247 page, London..

Nabarro, F. R. N. and De Villiers, H. L. 2018. The physics of creep: creep and creep-resistant alloys. CRC press, 350 page, UK.

Oliveira, J. P., Curado, T. M., Zeng, Z., Lopes, J. G., Rossinyol, E., Park, J. M. and Kim, H. S. 2020. Gas tungsten arc welding of as-rolled CrMnFeCoNi high entropy alloy. Materials and Design, 189: 6-12.

Patterson, T. 2008. Effects of internal oxidation on thermo-mechanical properties of atmospheric plasma sprayed CoNiCrAlY coatings, MSc. Thesis, University of Central Florida, 59 page, USA.

Pawlowski, L. 2008. The science and engineering of thermal spray coatings. John Wiley and Sons, 656 page, USA.

Picas, J. A., Ruperez, E., Punset, M. and Forn, A. 2013. Influence of HVOF spraying parameters on the corrosion resistance of WC–CoCr coatings in strong acidic environment. Surface and Coatings Technology, 225: 47-57.

Rakesh, G., Singh, S. B. and Grewal, J. S. 2010. Surface engineering and detonation gun spray coating. International Journal of Engineering Studies, 2(3): 351-357.

Rocha, A. D. C., Rizzo, F., Zeng, C. and Paes, M. P. 2004. Duplex Al-based thermal spray coatings for corrosion protection in high temperature refinery applications. Materials Research, 7: 189-194.

Rocha, A. D. C., Rizzo, F., Zeng, C. and Paes, M. P. 2004. Duplex Al-based thermal spray coatings for corrosion protection in high temperature refinery applications. Materials Research, 7: 189-194.

Ross, R. B. 2013. Metallic materials specification handbook. Springer Science and Business Media, 830 page, USA.

Rybin, D. K., Batraev, I. S., Dudina, D. V., Ukhina, A. V. and Ulianitsky, V. Y. 2021. Deposition of tungsten coatings by detonation spraying. Surface and Coatings Technology, 409: 3-12.

Sahab, A. R. M. 2008. The effect of plasma spray variables on the development of ceramic coatings, M. Sc. Thesis, Universiti Sains Malaysia, 140 page, Malaysia.

Samal, S. 2017. Thermal plasma technology: The prospective future in material processing. Journal of Cleaner Production, 142: 3131-3150.

Sarikaya, O. 2005. Effect of some parameters on microstructure and hardness of alumina coatings prepared by the air plasma spraying process. Surface and Coatings Technology, 190(2-3): 388-393.

Satapathy, A. 2005. Thermal Spray Coating of Redmud on Metals. Doctoral dissertation, National Institute of Technology Rourkela, 156 page, India.

Spray, A. 2004. Thermal Spray Processes. Handbook of Thermal Spray Technology, 54: 3-9.

Starosta, R. 2008. Testing of regenerative thermal spraying Ni-Al alloy coatings. Journal of Polish CIMAC. Diagnosis, Reliability and Safety, 3(2): 155-161.

Surmenev, R. A. 2012. A review of plasma-assisted methods for calcium phosphate-based coatings fabrication. Surface and Coatings Technology, 206(8-9): 2035-2056.

Suryanarayana, C. and Grant, N. 1998. X-ray diffractionA Practical Approach. Plenum Press, 273 page, New York.

Tarasi, F., Medraj, M., Dolatabadi, A., Oberste-Berghaus, J. and Moreau, C. 2008. Effective parameters in axial injection suspension plasma spray process of alumina-zirconia ceramics. Journal of Thermal Spray Technology, 17(5): 685-691.

Tomaszek, R., Znamirowski, Z., Pawlowski, L. and Zdanowski, J. 2007. Effect of conditioning on field electron emission of suspension plasma sprayed TiO2 coatings. Vacuum, 81(10): 1278-1282.

Tuominen, J., Vuoristo, P., Mäntylä, T., Kylmälahti, M., Vihinen, J. and Andersson, P. H. 2000. Improving corrosion properties of high-velocity oxy-fuel sprayed inconel 625 by using a high-power continuous wave neodymium-doped yttrium aluminum garnet laser. Journal of thermal spray technology, 9(4): 513-519..

Turunen, E. 2005. Diagnostic tools for HVOF process optimization. VTT Technical Research Centre of Finland, 92 page, Finland.

Vardelle, A., Moreau, C., Akedo, J., Ashrafizadeh, H., Berndt, C. C., Berghaus, J. O. and Vuoristo, P. 2016. The 2016 thermal spray roadmap. Journal of thermal spray technology, 25(8): 1376-1440.

Vinson, J.R. 1999. Composite Material and their use in Structure. Applied Sciences publisher LTD, 280 page, London.

Viswanathan, R. and Dolbec, A. C. 1987. Life assessment technology for combustion turbine blades, 109(1): 115-123.

Voorwald, H. J. C., Souza, R. C., Pigatin, W. L. and Cioffi, M. O. H. 2005. Evaluation of WC–17Co and WC–10Co–4Cr thermal spray coatings by HVOF on the fatigue and corrosion strength of AISI 4340 steel. Surface and Coatings Technology, 190(2-3): 155-164.

Wielage, B., Wank, A., Pokhmurska, H., Grund, T., Rupprecht, C., Reisel, G. and Friesen, E. 2006. Development and trends in HVOF spraying technology. Surface and Coatings Technology, 201(5): 2032-2037.

Yin, S., Cizek, J., Suo, X., Li, W. and Liao, H. 2019. Thermal spray technology. Advances in Materials Science and Engineering, 2: 2-12.

Zhu, D. and Miller, R. A. 2004. Development of advanced low conductivity thermal barrier coatings. International Journal of Applied Ceramic Technology, 1(1): 86-94.

CURRICULUM VITAE

Personal Information

Name and Surname : Jalal Riyadh Nayyef NAYYEF

Education

MSc	Çankırı Karatekin University Graduat School of Natural and Applied Sciences Department of Physics	2020-2022
Undergraduate	Tikrit University College of Education for Pure Sciences Department of Physics	2014-2019